N2O5 at Water Surfaces: Binding Forces, Charge Separation, Energy Accommodation and Atmospheric Implications

Journal:	*Physical Chemistry Chemical Physics*
Manuscript ID	CP-ART-05-2018-003022.R1
Article Type:	Paper
Date Submitted by the Author:	10-Jun-2018
Complete List of Authors:	Hirshberg, Barak; Hebrew University of Jerusalem, Department of Chemistry Rossich-Molina, Estefania; Hebrew University of Jerusalem, Department of Chemistry Götz, Andreas; University of California San Diego, San Diego Supercomputer Center Hammerich, Audrey Dell; University of Illinois at Chicago, Chemistry Nathanson, Gilbert; University of Wisconsin Madison Bertram, Timothy; University of Wisconsin Madison Johnson, Mark; Yale University, Department of Chemistry Gerber, Robert; The Hebrew University of Jerusalem , Chemistry; University of California, Irvine,

N_2O_5 at Water Surfaces: Binding Forces, Charge Separation, Energy Accommodation and Atmospheric Implications

Barak Hirshberg[1], Estefanía Rossich Molina[1], Andreas W. Götz[2], Audrey D. Hammerich[3], Gilbert M. Nathanson[4], Timothy H. Bertram[4], Mark A. Johnson[5] and R. Benny Gerber[1,6]

1. The Institute of Chemistry and the Fritz Haber Center for Molecular Dynamics, the Hebrew University, Jerusalem 9190401, Israel.
2. San Diego Supercomputer Center, University of California, San Diego, La Jolla, California 92093, United States.
3. Department of Chemistry, University of Illinois at Chicago, Chicago, Illinois 60607, United States
4. Department of Chemistry, University of Wisconsin-Madison, 1101 University Avenue, Madison, Wisconsin 53706, United States
5. Department of Chemistry, Yale University, New Haven, Connecticut 06525, United States.
6. Department of Chemistry, University of California, Irvine, California 92697, United States.

Abstract

Processes of N_2O_5 in water media are of great importance in atmospheric chemistry, and have been the topic of extensive research for over two decades. Nevertheless, many physical and chemical properties of N_2O_5 at the surface or in bulk water are unknown, or not microscopically understood. This paper presents extensive new results on physical properties of N_2O_5 in or at the surface of water, with a focus on their microscopic basis. The main results are obtained using *ab initio* molecular dynamics and calculations of a potential of mean force. These include: (1) Collisions of N_2O_5 with water at 300 K lead to trapping at the surface, for at least 25 ps with 95% probability. (2) During that time, there is no hydrolysis, evaporation, or entry into the bulk of N_2O_5. (3) There is a charge separation between the NO_2 and NO_3 groups of N_2O_5, which fluctuates significantly with time. (4) Energy accommodation of the colliding N_2O_5 at the surface takes place within picoseconds. (5) The binding energy of N_2O_5 to a nanosize amorphous ice particle at 0 K is on the order of 15 kcal mol^{-1}, for the main surface site. The binding is due to one weak hydrogen bond, and to interactions between partial charges on the N_2O_5 and on water. (6) The free-energy profile was calculated for transporting N_2O_5 from the gas phase through the interface and into bulk water. The corresponding concentration profile exhibited a propensity for N_2O_5 at the aqueous surface. The free energy barrier for entry from the surface into the bulk was determined to be 1.8 kcal mol^{-1}.

The above findings are used for the interpretation of recent experiments. These are discussed with focus on implications to atmospheric chemistry.

I. Introduction

This study presents a theoretical investigation of the chemical and physical properties of N_2O_5 in water media. These properties provide an important background for understanding the heterogeneous atmospheric chemistry of N_2O_5. The tropospheric significance of N_2O_5 stems from its role as a nighttime reservoir for NO_x species,[1–4] which catalyze photochemical oxidation of volatile organic compounds (VOC) to form ozone.[3] Atmospheric NO_2 can react with ozone to form NO_3, which undergoes rapid photodissociation[5] during the day. However, during the night, NO_3 reacts with NO_2 to reversibly form N_2O_5.[6] As a result, nocturnal N_2O_5 serves as a temporary reservoir for NO_x, and thus its fate has significant implications for the abundance of atmospheric ozone, hydroxyl radicals, methane, and more.[7–9] In particular, model simulations by MacIntyre and Evans[9] show that variations in the reactivity of N_2O_5 in aqueous particles can result in up to approximately 12%, 15% and 25% losses in global tropospheric ozone, hydroxyl radical, and NO_x concentrations, respectively.

Much of the importance of N_2O_5 in the troposphere involves its interactions with water media ranging from continental and sea spray aerosol particles to the ocean surface. These particles can be liquid or solid and vary in size from very small water clusters[10] through nano-sized particles and up to ~10-100 μ m in diameter.[1,2] In this study, we present computational results for small and nanometric water clusters through extended liquid water surfaces to bulk water. The importance of N_2O_5-water interactions is evident from the fact that the main removal mechanism of N_2O_5 is through hydrolysis in aerosol particles to form nitric acid.[11–15] In addition to hydrolysis, N_2O_5 can react with halide-containing particles to form XNO_2 (X = Cl, Br, I), which results in the production of active halogen atoms in the troposphere.[15–19] Moreover, the composition of aqueous aerosol particles can be very rich, and include organic and biological constituents.[20] Here, we focus on the study of pure water systems to obtain a clear understanding of the fundamental interactions between N_2O_5 and water. The influence of additional ions and organic species will be addressed in the future.

Due to the important role of N_2O_5 in the atmosphere, it has been extensively studied both computationally and experimentally.[4,6,21–23] Computational studies have focused mainly on the structure of isolated N_2O_5[24–26] or on calculating stationary points along the reaction profile of N_2O_5 with a small number of water molecules.[27–35] Recently, Hammerich *et al.* performed the first molecular dynamics (MD) simulations of the reaction between Cl^- and N_2O_5 adsorbed on the surface of liquid water.[19] Their simulations showed the importance of charge fluctuations in N_2O_5 for reactivity. Gaston and Thornton recently estimated the half-life time for hydrolysis of N_2O_5 to be on the microsecond timescale.[36] Thus, the direct observation of hydrolysis is beyond the scope of this study. Here, we focus on the physical interactions that precede hydrolysis but are nonetheless important for understanding the factors that control the interfacial reactivity of N_2O_5 on aerosols.

This paper presents results according to several themes: First, we investigate collisions of N_2O_5 with the surface of liquid water. MD simulations can be used to study in detail the dynamics of molecular collisions on liquid and solid surfaces and, in particular, for analyzing the physical interactions between atmospherically-important trace gases and water surfaces[37]. This approach has also been very successful in studying chemical reactions of atmospherically-relevant molecules on water surfaces.[38–45] In addition, simulations can provide information complementary to recent molecular beam scattering experiments, which examined the desorption kinetics of N_2O_5 and energy transfer to ice surfaces[46] and the effect of salt concentrations and of different surfactants on the surface reaction between N_2O_5 and salty glycerol solutions.[47] Classical trajectories can also provide answers to important questions at the molecular level: What fraction of impinging N_2O_5 molecules become momentarily trapped at the surface? How fast, and to what extent, is the kinetic energy of N_2O_5 accommodated at the surface? Does the surface of water create a significant charge separation in the N_2O_5 molecule?

A second theme is the interaction between N_2O_5 and water clusters, in particular nanoclusters composed of 10-20 water molecules. Several previous studies addressed the structure, energetics and reaction pathways of N_2O_5 with water clusters containing up to six water molecules.[27–34] Here, we focus on results for water clusters of nanometer sizes, which are close to the size of the smallest measured atmospheric aerosols (~2 nm).[1,2] Studies of cluster structures offer a powerful framework for evaluating the nature and strength of N_2O_5-water hydrogen bonds, as well as water network-mediated distortions in the N_2O_5 charge distribution and structure.[48] Large enough clusters can also be used as a bridge to discern the differences between N_2O_5 at the surface of a cluster and in “encapsulated” solvated structures.

A third important theme is the thermodynamics of adsorption and evaporation of N_2O_5 from the surface of water compared with the solubility of N_2O_5 in bulk water. The solubility of N_2O_5 plays an important role in atmospheric models of N_2O_5 reactivity.[21] Despite its significance, it has not yet been directly measured and only estimates are currently available, ranging from 1 to 10 M atm^{-1}.[49–51] MD simulations can be used to calculate a potential of mean force (PMF), which provides a theoretical estimate of the solubility of N_2O_5.

The last theme of this study is the connection between physical properties and their atmospheric significance. Several questions can be addressed in this context: How do parameters such as charge separation and hydrogen bonding affect the reactivity of N_2O_5 at the surface compared with the bulk? Do the timescales for energy accommodation and charge separation suggest that reactivity at the surface is possible and should be addressed in atmospheric models?

The structure of the paper is as follows: Section II discusses N_2O_5 collisions with pure liquid water, while Section III describes the interaction of N_2O_5 with water clusters. In Section IV, the thermodynamics of N_2O_5 adsorption on the surface of water and solvation in bulk water are discussed. Section V discusses the atmospheric implications of the results given in this paper, summarizes the work and presents the conclusions.

II. Scattering, trapping and energy accommodation of N_2O_5 at water surfaces

As discussed in the introduction, the physical properties of N_2O_5 on the surfaces of aerosols (binding energy, hydrogen bonding and rate of energy transfer upon collision) are important to understand the reactivity of N_2O_5 in the troposphere. However, these physical interactions have been far less studied both experimentally and theoretically, particularly at the air/water and air/ice interface. Recently, Lejonthun *et al.*[46] investigated the scattering of N_2O_5 from the surface of ice using molecular beams and characterized the desorption kinetics and energy transfer to the ice surface at temperatures between 93 and 180 K. N_2O_5 was scattered from the surface with mean incident energy of 21.4 kcal mol^{-1} and the surface collision was found to be highly inelastic with significant kinetic energy transfer to the surface of ice. The binding free energy to pure ice was found to be 8.3 ± 0.5 kcal mol^{-1}. This value is similar to the prediction of McNamara and Hillier,[34] who determined the binding energy of N_2O_5 with small “ice-like” water clusters to be 6.0 and 7.1 kcal mol^{-1} for clusters with 4 and 6 water molecules, respectively. These values are, however, lower than a previous estimate by Tabazadeh and Turco[52] of the energy of adsorption on ice of 12.1 kcal mol^{-1}. Here, we present MD simulations of the scattering of N_2O_5 from an extended surface of liquid water. The simulations provide insights into collisional energy transfer between N_2O_5 and surface water molecules, the trapping of N_2O_5 on the surface, and hydrogen bonding and charge fluctuations of adsorbed N_2O_5.

(a) Model systems and methodology

We follow procedures similar to the simulations used by the Gerber group in several previous publications[19,40,53] to describe chemical reactions on water. The surface of liquid water was modeled by 72 water molecules in a 13.47 x 15.56 x 40 Å^3 rectangular box. Periodic boundary conditions were employed in x and y but not in the z direction. The liquid slab was equilibrated using a Nosé-Hoover massive thermostat[54] at 300 K for 50 ps. Using the same analysis as in Murdachaew *et al.*[40] the thickness and density of the liquid slab were determined to be 9.9 Å and 1.03-1.06 g cm^{-3}.

For calculations of N_2O_5 in bulk liquid water, a cubic box with side-length of 12.73 Å containing 64 water molecules was generated using the solvate tool in GROMACS[55]. Then, one water molecule at the center of the box was replaced with an N_2O_5 molecule. The system was first coarsely equilibrated at 300 K for 15 ps using a Nosé-Hoover massive thermostat[54] with a 1 fs time constant. Then, the velocities of the system were resampled from a Maxwell-Boltzmann distribution at the same temperature and the system was again equilibrated at 300 K for an additional 5 ps with a time constant of 1000 fs. Upon equilibration, the trajectories were continued for an additional 20 ps for collection of data included in this paper. The MD simulation of isolated gas-phase N_2O_5 used an optimized molecular structure as the initial configuration for an NVT simulation at 300 K in a cubic box of side-length of 25 Å. The initial velocities were sampled from a Maxwell-Boltzmann distribution for the same temperature and the simulation ran for longer than 12 ps. Panels (b) and (c) in Figure 1 depict the models used for N_2O_5 in bulk liquid water and N_2O_5 scattering simulations.

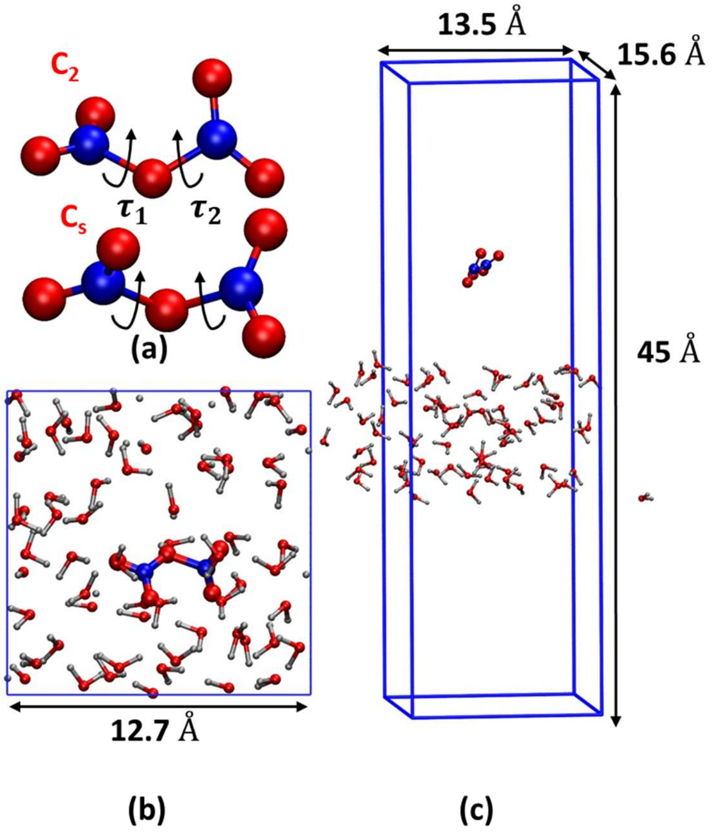

Figure 1. (a) Optimized structures for two conformers of N_2O_5 at the ωB97X-D/aug-cc-pVTZ level of theory. The dihedral angles τ_1 and τ_2 between the central N-O-N plane

and the two NO_2 groups are also marked. See Figure S3 in SI for full structural parameters. (b) Model for N_2O_5 in bulk water simulations. (c) Model for N_2O_5 scattering from liquid water simulations showing only one of two initial configurations (see Section II(b) for more details).

All optimizations and MD simulations were performed using the QUICKSTEP module[56] within CP2K 3.0.[57] Density functional theory (DFT) employing the Perdew-Burke-Ernzerhof (PBE) functional[59] with an empirical dispersion correction (PBE-D3) due to Grimme[60,61] was used with a double-zeta valence polarization basis-set (DZVP-MOLOPT-SR)[62] and the Goedecker-Teter-Hutter (GTH) pseudopotentials.[63] Long-range electrostatic interactions are treated using the Martyna-Tuckerman algorithm.[64] Accurate description of dispersion interactions is essential for investigation of N_2O_5 interactions with the surface of water and in bulk water. The cutoff for the plane-waves basis-set was 320 Ry. The time step for all MD simulations was 0.5 fs and all hydrogen atoms were replaced by deuterium to allow for a larger time step. This is justified since quantum effects are not expected to be significant for the properties reported in this section.

(b) Scattering simulations

Prior to performing the scattering simulations, an optimized N_2O_5 molecule was placed approximately 6 Å above the center of the equilibrated liquid slab and the z dimension of the box extended to 45 Å (see panel (c) in Figure 1). The system was then equilibrated for 2 ps at 300 K. During equilibration, the center of mass (COM) of N_2O_5 was harmonically constrained (using a spring constant of 0.1 Hartree bohr^{-2}) so the molecule could rotate and equilibrate vibrationally but could not move towards the surface. A scan of the potential energy surface (PES) as a function of the distance between N_2O_5 and the water slab confirmed that the interaction between the surface and N_2O_5 is negligible at this chosen distance. Two structures, approximately representing N_2O_5 parallel to the water surface and N_2O_5 perpendicular to the surface, were taken from the end of the 2 ps equilibration and used as initial configurations for the scattering simulations. In each trajectory, an additional COM velocity in the z direction for the N_2O_5 molecule was sampled from the Maxwell-Boltzmann distribution for 300 K using the total mass of N_2O_5. Then, the COM constraint was removed and 20 trajectories, 10 for each initial relative configuration of N_2O_5 with respect to the surface, were initiated and run for 20-25 ps. The first 5 ps of each trajectory were discarded in the probability distribution analyses reported in this section.

Trapping, energy accommodation and entry. All but one of the 20 trajectories discussed above show that after N_2O_5 hits the surface it becomes trapped at the surface for at least 20 ps. The one exception was a trajectory which showed desorption of N_2O_5 from the surface after approximately 19 ps. These results correspond to a trapping probability of 95% per collision. This nearly complete trapping is in accord with gas-liquid scattering experiments involving collisions of N_2O_5 with salty glycerol and salty water[47]. These studies show that unreacted N_2O_5 molecules depart from the surface with a Boltzmann distribution characteristic of the temperature of the liquid, implying that they first become momentarily trapped at the surface before desorbing.

A plot of the COM velocity components, COM distance along the z axis of N_2O_5 and the boundaries of the water slab from a representative trajectory are given in Figure 2. Several selected snapshots from the same trajectory are also shown. N_2O_5 is initially out of the range of interaction with the water surface, so it moves towards the surface with constant velocity. Once the N_2O_5 molecule enters the interaction region it starts accelerating until it impacts the surface. The molecule then becomes trapped on the surface but has relatively high mobility. The molecule explores significant portions of the surface of water and also fluctuates and rotates with respect to the surface over a 20-25 ps timescale.

The energy accommodation of N_2O_5 is analyzed through fluctuations in its COM velocity components, shown in Figure 2. Initially, the x and y components are equal to zero while the z component is negative and defines the relative collision energy. After accelerating towards the surface and within a few ps after impact, the COM velocity fluctuations for all three components become similar in magnitude and also similar to the COM fluctuations of N_2O_5 thermalized in bulk liquid water at 300 K (not shown). These observations suggest that energy transfer and accommodation occur on a fast timescale of several ps. While this analysis is only qualitative in nature it provides a correct physical timescale for energy accommodation. Different trajectories showed similarly fast energy accommodation.

Lastly, we address the probability of entry into the bulk. In all trajectories, N_2O_5 stayed very close to the surface of liquid water (with the exception of 1 trajectory that showed desorption, as discussed above) and no absorption into bulk liquid water was seen on a timescale of 20-25 ps. Recently, Murdachaew *et al.* calculated the trapping and accommodation of a related molecule, NO_2, on the surface of liquid water.[37] Using empirical potentials, they ran scattering trajectories for 90 ps. In their simulations, only 1% of trajectories were directly scattered, 53% were trapped at the surface for a significant period of time (of which about 20% were eventually desorbed and the rest remained on the surface) and 46% were absorbed into the bulk. Our results are in qualitative agreement with their simulations: We see no direct scattering, 1 trajectory that shows trapping and subsequent desorption and we mostly observe that N_2O_5 molecules remain trapped on the surface. Absorption into the bulk is not seen mainly because N_2O_5 is significantly larger than NO_2 and thus entry into bulk water is expected to take longer. In addition, the use of ab initio potentials is demanding computationally and mandates shorter trajectories than when empirical potentials are used. However, these empirical potentials cannot accurately describe the charge fluctuations within the N_2O_5

molecule, which are discussed in the next paragraph, unless a polarizable force field is developed for this purpose. Lastly, we note that, as expected, no hydrolysis is seen on a 20 ps timescale. This is not surprising and emphasizes the need for enhanced sampling techniques, such as metadynamics,[65] for studying the hydrolysis reaction. Work in this direction is underway.

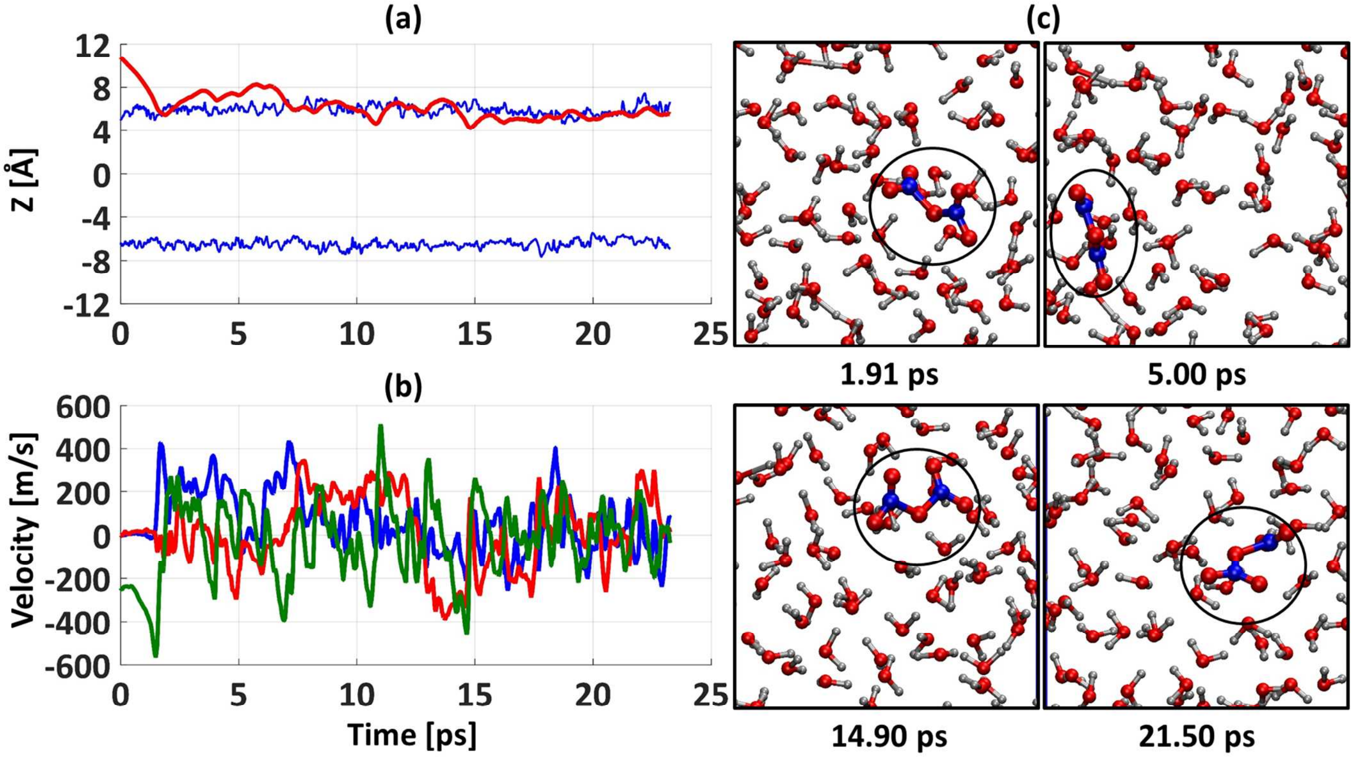

Figure 2. (a) Position along the z direction (normal to the water surface) during a representative trajectory. The red curve represents the COM of N_2O_5 and the blue curves the topmost and bottommost water molecules, which approximates the instantaneous slab thickness. (b) The COM velocity components for N_2O_5 along the same trajectory. The blue, red and green curves represent the x, y and z COM velocity components, respectively. (c) Snapshots from the same trajectory showing the movement of N_2O_5 along the surface.

Charge separation and charge fluctuations. Our *ab initio* molecular dynamics (AIMD) simulations provide insight into the charge fluctuations within the N_2O_5 molecule after it collides with the water surface and becomes trapped. Hammerich *et al.* have shown previously that the fluctuations of charge within the N_2O_5 molecule are a good indicator for the possibility of reaction with Cl^-.[19] Moreover, it has been suggested in the literature by several authors that N_2O_5 must undergo significant charge separation in the transition-state structure for hydrolysis to occur.[27,28,34] In one suggested mechanism[66], N_2O_5 reactions is initiated by ionization of N_2O_5 to form solvated NO_2^+ and NO_3^-, although this ionization has not been directly observed and is still under debate.[28] The Mulliken partial charges on the NO_2 and NO_3 fragments of N_2O_5 during a representative trajectory are given in Figure 3 along with the same analysis performed for isolated gas phase N_2O_5 and N_2O_5 in bulk water. These charges are calculated by arbitrarily dividing the N_2O_5 molecule into NO_2 and NO_3 fragments (see inset in Figure 3), following Hammerich *et al.*,[19] who showed that the charge fluctuations on these fragments increase before reaction with Cl^- occurs. Comparing the charges on each fragment in the gas phase and on the surface, it is clear that some charge fluctuations occur in the gas phase as well, simply due to the thermal motion of the atoms. However, the charge separation is increased on the surface of liquid water. A similar enhancement, in comparison to the gas-phase, is seen for N_2O_5 in bulk water.

The lower panel in Figure 3 shows the probability distribution as a function of partial charge on the NO_3 moiety of N_2O_5, calculated from the scattering trajectories. The distribution for the NO_2 fragment approximately mirrors that of NO_3. Only the last 15 ps of each trajectory are taken into account in the analysis. It is seen that the most probable charge on the $NO_2^{\delta+}$ and $NO_3^{\delta-}$ fragments is ± 0.21, respectively. We note that these charge fluctuations are already obtained in the vicinity of the water surface and are similar in magnitude to the fluctuations observed in the simulations of Hammerich *et al.*[19] where N_2O_5 was initially adsorbed on the surface of water. From these distributions we see that if a rare charge fluctuation is indeed required for hydrolysis, it is similarly likely to occur on the surface as in bulk. However, the charge fluctuations are probably not sufficient and a suitable reorganization of the surface water molecules in the vicinity of N_2O_5 is also required. Based on our simulations, we speculate that this rearrangement of the water molecules occurs on a longer timescale than the charge fluctuations. In other words, the charge fluctuations may be necessary but are not sufficient for reactivity. Some charge fluctuation occurs almost immediately when N_2O_5 is trapped on the surface.

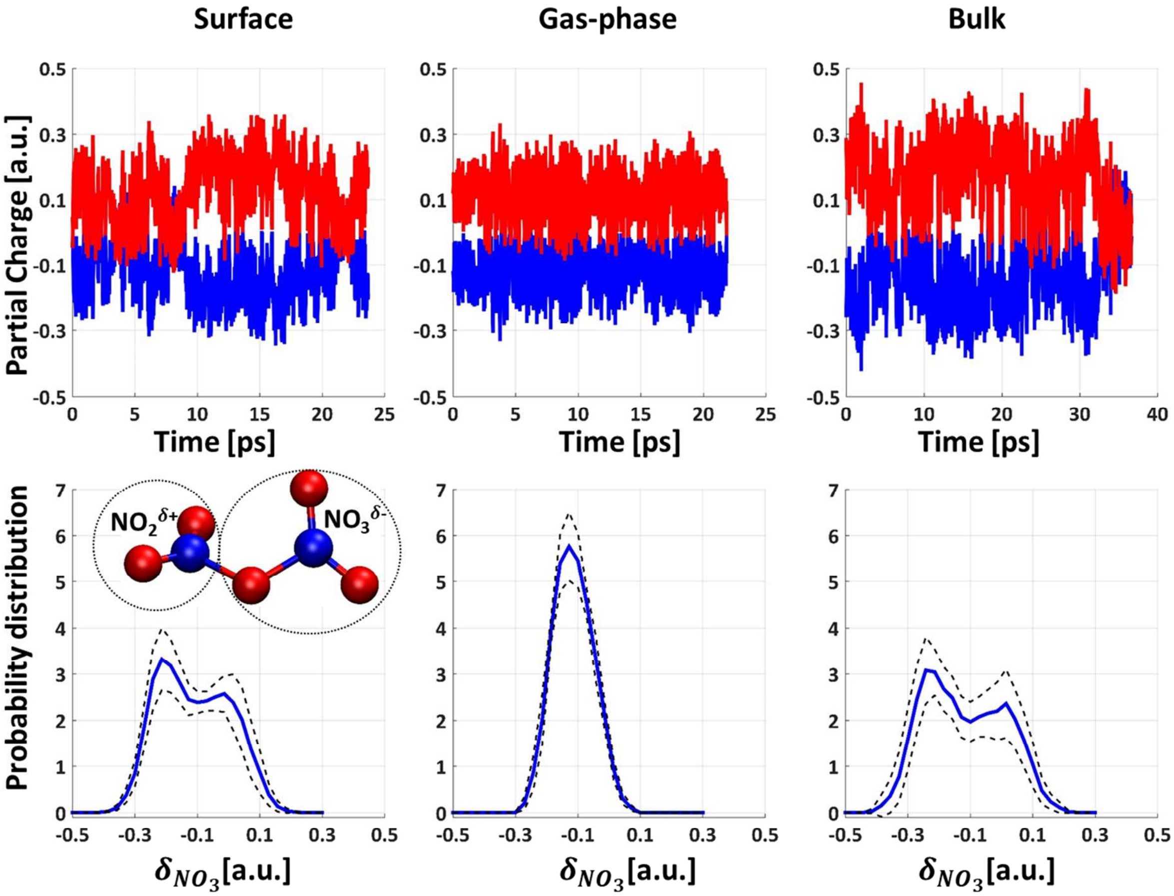

Figure 3. Analysis of charge distribution of N_2O_5 on the surface of liquid water, in the gas-phase and in bulk. The top panel shows the charge on the NO_2 (red) and NO_3 (blue) fragments of N_2O_5 as defined in the inset. The bottom panel shows the probability distribution for the NO_3 fragment to have a certain partial charge, obtained from averages over all trajectories for a given system. The probability distribution for NO_2

approximately mirrors that of NO_3 and is not shown. Blue curve presents the distribution while the dashed black line presents two standard deviations from the mean distribution.

Hydrogen bonding. The hydrogen bonding of N_2O_5 to surface water molecules was analyzed based on geometric criteria. We define a hydrogen bond if the donor-acceptor distance is smaller than 3.2 Å and the D-H···A angle (where D stands for hydrogen bond donor and A stands for hydrogen bond acceptor) is larger than 140°, following Murdachaew *et al.*[40] Through this analysis the number of hydrogen bonds between N_2O_5 and the water surface as a function of time was determined using the VMD software[67] and is given in the upper panels of Figure 4 for representative trajectories. For most trajectories, the number of hydrogen bonds is found to be between no bonds to two bonds (with the exception of a single trajectory showing three hydrogen bonds for a very brief period of time). The lower panels in Figure 4 present the probability distributions obtained by taking all trajectories into account. The most probable value was no hydrogen-bonds. The small number of bonds in Figure 4 reflects the fact that N_2O_5 is not well solvated by surface water molecules, which allows it to explore many surface sites rather than sticking to one binding site. For comparison, we carried out the same analysis for N_2O_5 in bulk water. The results show similar trends. The number of hydrogen bonds is slightly larger and ranges mostly between zero and three, with just a single trajectory showing four hydrogen bonds for a very short time (not shown). Despite this difference, the most probable number of hydrogen bonds in all trajectories is still zero, with only a single trajectory showing approximately equal probability for no hydrogen-bonding and 1 hydrogen bond. These results indicate that N_2O_5 is also not well solvated in bulk water, but it does have slightly more possibilities for creating short-lived hydrogen bonds than on the surface.

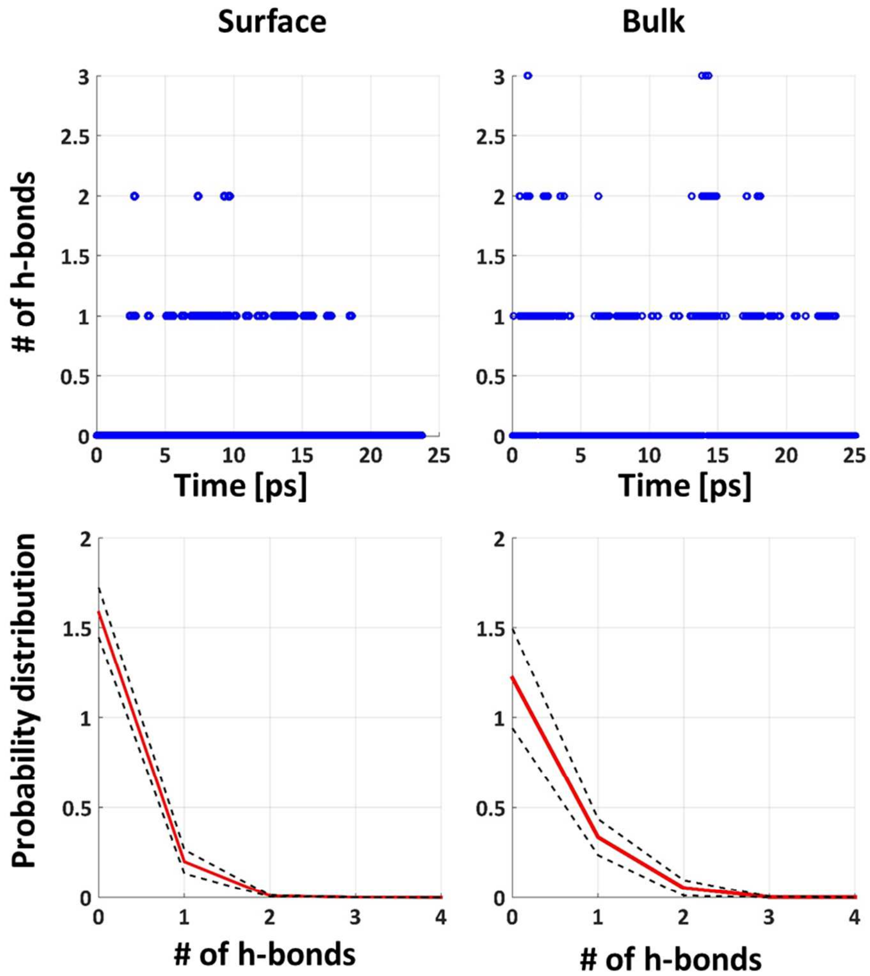

Figure 4. Analysis of the number of hydrogen bonds between N_2O_5 and the surface of liquid water or in bulk liquid water. The top panel shows the number of hydrogen bonds for representative trajectories. The bottom panel presents the probability distribution as a function of the number of hydrogen bonds, obtained from averaging over all trajectories for a given system. Red curve gives the distribution while the dashed black line presents two standard deviations from the mean distribution.

Structural changes. Grabow *et al.* reported previously[26] that at the MP2/6-31G* level of theory two minimum conformers exist on the PES for N_2O_5. Jitariu and Hirst found similar results at the B3LYP/6-311G* level of theory.[25] One conformer has C_2 symmetry and was observed experimentally[26,68,69] using both microwave spectroscopy and electron diffraction. The other conformer belongs to a C_s point group and was not detected experimentally.

We have optimized the structure of the two conformers using DFT, employing the long-range corrected hybrid density functional with a dispersion correction by Head-Gordon *et al.*,[70] ωB97X-D, and Dunning's augmented triple-zeta basis set with polarization functions (aug-cc-pVTZ).[71] Additionally, we compared our calculations with the B3LYP-D3[72,73]/aug-cc-pVDZ[71] level of theory (see Section III). The results are consistent for both levels of theory (bond length differences < 0.05 Å). The optimized structures of the two conformers are shown in panel (a) of Figure 1 and in the SI. Results at this level of theory are in nice agreement with the experimental values for the C_2 conformer, as can be seen in Figure S3 of the SI. The two main structural differences between the conformers are the central N-O bond lengths and the dihedral angles, denoted by τ_1 and τ_2, formed between the central N-O-N plane and each one of the adjacent NO_2 groups (see Figure 1(a)). While for the C_2 conformer both N-O bond lengths are equal to 1.47 Å, in the C_s conformer one bond length is 1.44 Å while the other is 1.51 Å. In addition, the dihedral angles τ_1 and τ_2 are identical and equal to 34° for the C_2 conformer but are 90° and 0° in the C_s conformer.

We wish to examine if transitions between the two conformers occur at the surface of water. In the gas phase, the isomers are almost degenerate in energy (< 0.1 kcal mol^{-1}) at the ωB97X-D/aug-cc-pVTZ level of theory and it is of interest whether water interacts preferentially with one conformer. Figure 5 shows the value of one dihedral angle in a representative scattering trajectory and the probability distribution for the dihedral angle, obtained by taking all trajectories into account. The results for the other dihedral angle are not shown but the probability distributions are very similar. This, and the fact that the probability distribution has only minor contributions at 90°, shows that the C_2 conformer is observed more often than the C_s isomer at the water surface. We note that the scattering trajectories are initialized from the C_2 conformer but the molecule is equilibrated before collision without any symmetry constraints (see Section II(b)). For comparison, we calculated the dihedral angle as a function of time for isolated gas-phase N_2O_5 and N_2O_5 in bulk water, which are also shown in Figure 5. Despite being degenerate in energy, the C_s isomer was not observed even in the gas phase, which suggests a barrier for conformational changes.

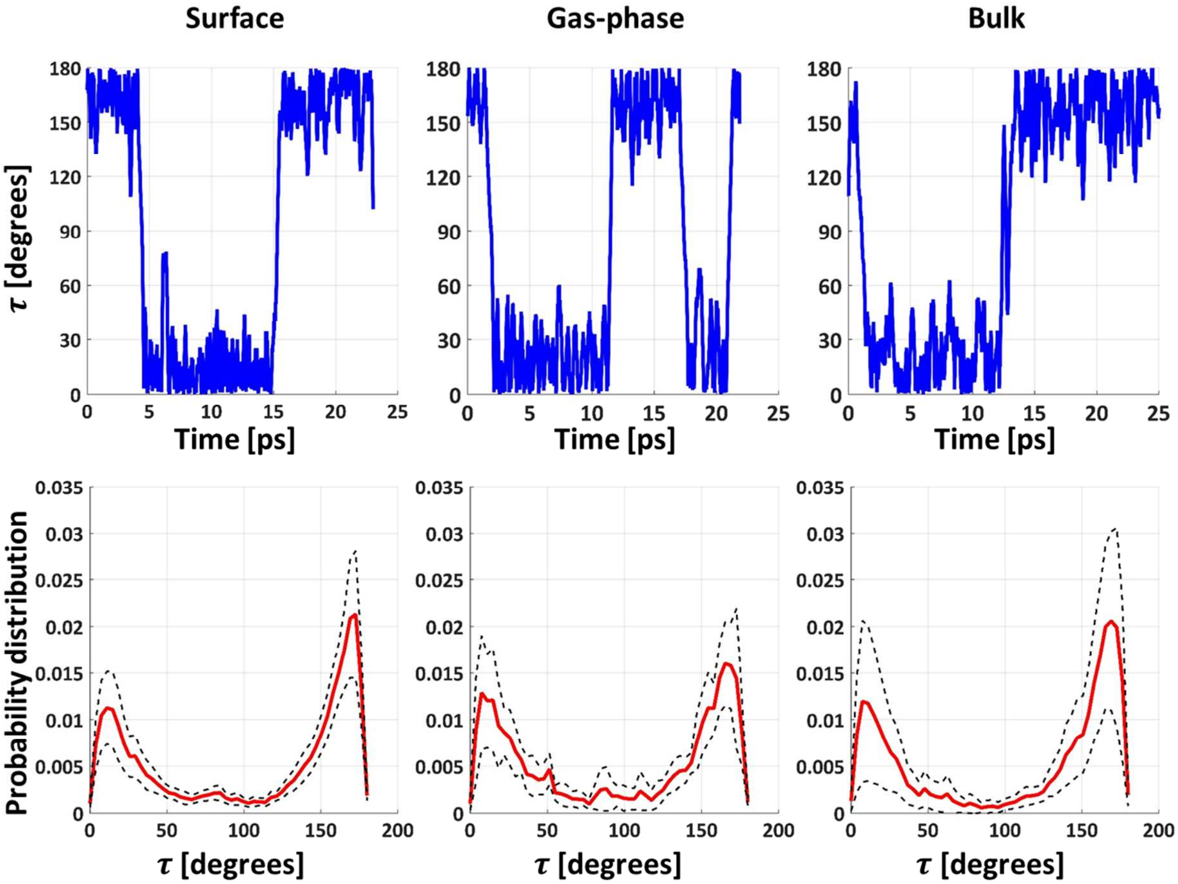

Figure 5. Analysis of one dihedral angle of N_2O_5 (see Figure 1(a)) at the surface of liquid water, in the gas-phase and in bulk. Top panel presents the dihedral angle along representative trajectories. Bottom panel presents the probability distribution as a function of τ, obtained from averaging over all trajectories for a given system. Red curve refers to the mean distribution while the dashed black line refers to two standard deviations from the mean. The results for the second dihedral angle for the probability distribution are very similar, and are not shown.

III. $N_2O_5\cdot(H_2O)_n$ clusters: structures, binding interactions and charge separation

Clusters of increasing size are useful systems for studying interactions of N_2O_5 and water both experimentally and theoretically.[10] In this section, we study clusters of N_2O_5 with 1-20 water molecules. The benefit of using small model systems is that they allow the use of high levels of theory that are computationally too expensive for the extended water surface discussed in the previous section. To gain a molecular level understanding of the solvation of N_2O_5 by water, certain molecular properties such as equilibrium geometries, binding energies and harmonic frequencies of the clusters are important. A minimum in the potential energy surface corresponds to an equilibrium geometry of a cluster, and provides structural information about the cluster and the interactions between N_2O_5 and different configurations of the surrounding network of water molecules. More specifically, variations in the water network lead to different local electric fields acting on the solute.[74,75] Moreover, analyzing different minimum energy structures allows exploration of transient effects in the liquid.[76,77] Lastly, the evolving solvent effect can be investigated by analyzing clusters of increasing size and the subsequent changes in N_2O_5 bonding.

Our approach to studying the hydration of N_2O_5 utilizes neutral $N_2O_5\cdot(H_2O)_n$ clusters with $n = 1, 2, 3, 4, 6, 10, 15, 20$. Amorphous cluster structures were built in a systematic way with the Packmol[78] software. First, using the optimized structures of isolated N_2O_5 and H_2O, we constructed amorphous clusters by randomly adding water molecules to N_2O_5 up to a desired size. As discussed in Section II, N_2O_5 can adopt two different nearly-degenerate conformers with C_2 and C_s symmetries. Thus, for a given n we considered two initial structures for the $N_2O_5\cdot(H_2O)_n$ clusters, one for each conformer. Then, the initial structures were optimized using Gaussian09 software[79] without imposing symmetry constraints. The optimized structures were found to be local minima with no imaginary frequencies. The amorphous structures are not global minima on the PES. However, considering several minima structures represent a local environment that can serve as models for liquid water and can thus be compared to the calculations of Section II.[76,77]

The partial charge on each atom was calculated by NBO[80] and binding energies were calculated and corrected for basis-set superposition error using the counterpoise correction.[81] We used DFT with the hybrid functional B3LYP,[72,73] Grimme's D3 correction for dispersion[60] and Dunning's aug-cc-pVDZ basis set[71] for all calculations, in order to incorporate dispersion effects.

(a) Cluster structures

Several theoretical studies of $N_2O_5{\cdot}(H_2O)_n$ structures with water clusters are available in the literature. Hanway and Tao[30] calculated the equilibrium structures for $N_2O_5{\cdot}(H_2O)_{n=1,2}$ using DFT at the B3LYP/6-31+G(d), B3LYP/6-311++G(d,p) and MP2/6-31+G(d) levels of theory. Snyder *et al.*, also studied the $N_2O_5{\cdot}(H_2O)_{n=1\text{-}4}$ clusters using B3LYP/6-31+G(d).[27] McNamara and Hillier[34] presented structural results using DFT with the B3LYP functional and 6-311++ G(d, p) basis set for $N_2O_5{\cdot}(H_2O)_n$ clusters for n = 1-6 and reported binding energies that range from 3.98 to 20.37 kcal mol^{-1}. High level electronic structure calculations for $N_2O_5{\cdot}(H_2O)_n$ clusters for pure water and $n > 6$ are not available in the literature. In the present study, we focus on the equilibrium structures for N_2O_5 on amorphous $(H_2O)_n$ clusters, their stability, charge distribution and binding energies for much larger clusters of n = 10, 15 and 20. In the SI we present the structural parameters and relative energies for the clusters with n = 1-6, which are in agreement with previous studies.

Note that hereafter, C_2 and C_s notations correspond to the geometry of N_2O_5 molecules before they are subjected to the optimization procedure described above. The extent to which the initial geometry and charge distribution are conserved or distorted is a direct consequence of their solvation by water. We will describe the changes in dihedral angles, defined in Figure 1, in order to determine if N_2O_5 has a preference for the C_2 or C_s conformation. In addition, we analyze how water solvation changes the charge distribution within N_2O_5 and the length of the two central N-O bonds to evaluate the tendency of N_2O_5 to form NO_2^+-NO_3^-. Henceforth, we use the term "surface" clusters when N_2O_5 is solvated at the surface, and "encapsulated" clusters when it is clear that the N_2O_5 molecule is surrounded by several water molecules. From our study, we observe that for $n < 20$, there are only "surface" clusters due to an insufficient number of water molecules to solvate the N_2O_5.

N_2O_5·$(H_2O)_n$, $n = 10$ and $n = 15$. Figure 6 shows the amorphous local minima structures for clusters containing 10 and 15 water molecules that were obtained from an initial C_s structure for N_2O_5. The geometry of the isolated C_s conformer is also presented for reference. As was mentioned in Section II, the dihedral angles for the isolated C_s isomer are equal to 90° and 0°. In addition, the two central N-O bonds are not equal as in the C_2 conformer. Using the B3LYP functional we find that the two central N-O bonds are equal to 1.56 Å and 1.45 Å. The optimized structure for $n = 10$ shows several differences, in comparison to the isolated molecule. First, the dihedral angles are equal to 21° and 19° which is significantly lower than the value for isolated C_s. In addition, the central N-O bonds become slightly closer in length (1.54 and 1.48 Å). Since the C_2 isomer has 2 equal central N-O bonds and $\tau_1 = \tau_2 \approx 30°$ at this level of theory, one can think of this structure as intermediate between the initial C_s and C_2 geometries. For $n = 15$, the dihedral angles also change significantly (47° and 17°), but not as much as for $n = 10$, and the two central N-O bond lengths differ more than in the case of isolated C_s N_2O_5 (1.59 and 1.43 Å).

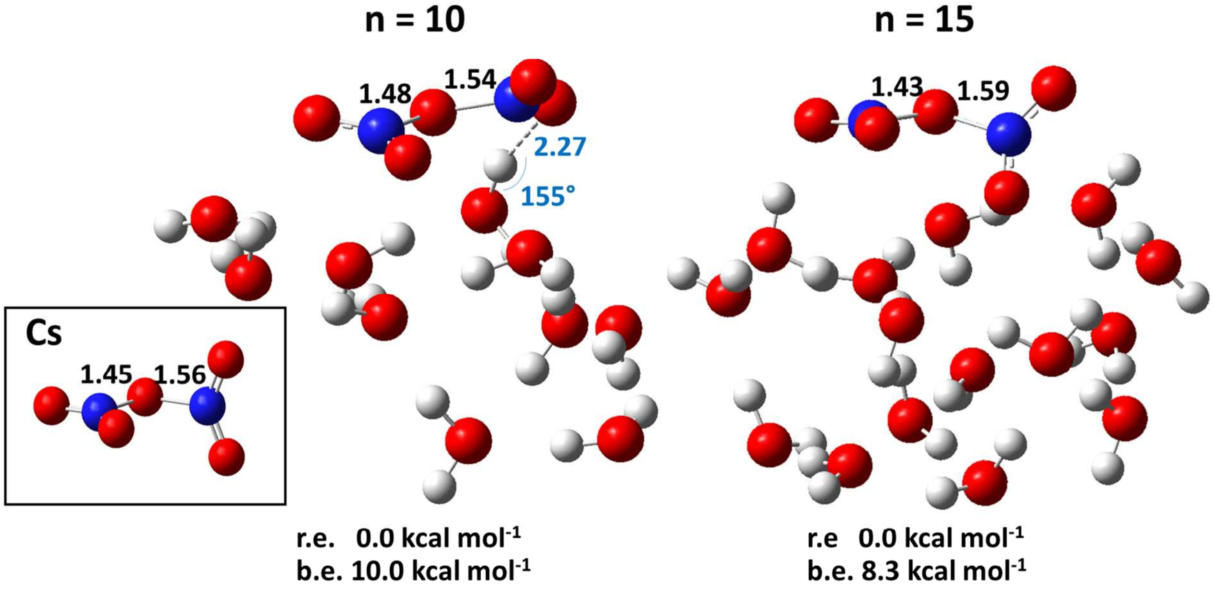

Figure 6. Amorphous local minimum structures for $N_2O_5{\cdot}(H_2O)_n$, *n* = 10 and *n* = 15. The structures were obtained from optimization of initial structures where N_2O_5 had C_s symmetry. Relative energies (r.e.), compared to lowest energy structure for each size, and binding energies (b.e.) are given below each structure. Bond lengths of the central N-O bonds are given in black and hydrogen-acceptor distances and hydrogen bond angles are given in blue. The structure of isolated C_s N_2O_5 is given in the inset.

Figure 7 gives the optimized amorphous structures for *n* = 10 and *n* = 15 that were obtained from initial clusters with the C_2 conformer of N_2O_5, as well as the structure of the isolated C_2 conformer for comparison. These clusters are less stable that the corresponding clusters in Figure 6 by 6.3 and 7.7 kcal mol^{-1}, respectively. Here, we see that the geometry of N_2O_5 is highly distorted by the presence of water; one central N-O bond is shortened while the other central N-O bond is elongated significantly, reducing its strength. For both the *n* = 10 and *n* = 15 clusters, N_2O_5 becomes more planar than the isolated C_2 structure. However, the effect is most pronounced for 10 water molecules, with the dihedral angles being 12° and 16°.

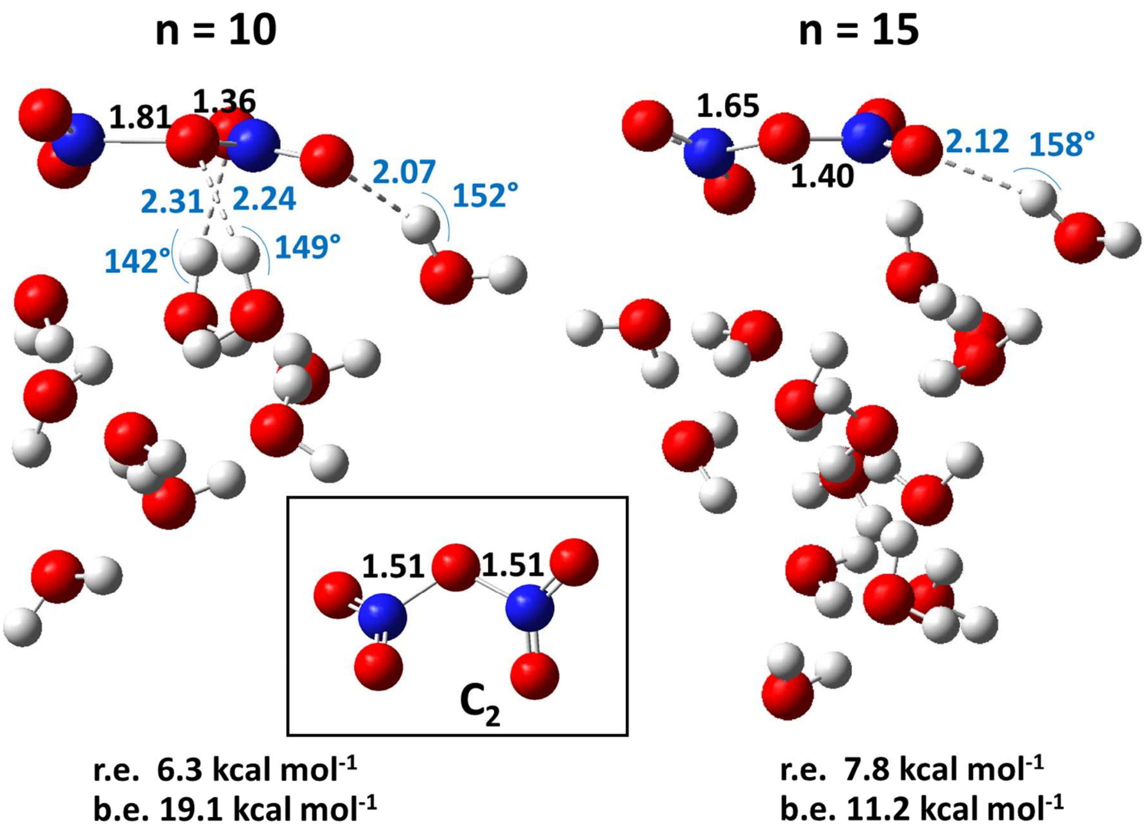

Figure 7. Higher-energy structures for $N_2O_5{\cdot}(H_2O)_n$, $n = 10$ and $n = 15$. The structures were obtained from optimization of initial clusters where N_2O_5 had C_2 symmetry. Relative energies (r.e.), compared to lowest energy structure for each size, and binding energies (b.e.) are given below each structure. Bond lengths of the central N-O bonds are given in black and hydrogen-acceptor distances and hydrogen bond angles are given in blue. The structure of isolated C_2 N_2O_5 is given in the inset.

From the analysis of the $n = 10$ and $n = 15$ amorphous clusters we conclude that, for the local minima structures studied here, N_2O_5 undergoes geometric distortions in the presence of water. We summarize the qualitative changes in Figure 8: Arrows pointing up denote an increase in the distance of a bond or amplitude of angle, while arrows pointing down denote a decrease in a value of distance or angle. In addition, N_2O_5 solvation by 10 water molecules produces more geometrical distortions than solvation by 15 water molecules, independent of the initial N_2O_5 structure.

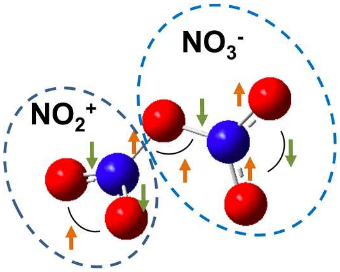

Figure 8. Qualitative description of changes in the length of the bonds and angles in the N_2O_5 molecule in the presence of 10 and 15 water molecules, in comparison to the gas-phase structure. Arrows pointing up denote an increase in the distance of a bond or amplitude of angle, while arrows pointing down denote a decrease in a value of distance or angle.

$N_2O_5 \cdot (H_2O)_{20}$. For these nano-size amorphous clusters, one can speak of two categories of structures: Those with the N_2O_5 molecule on the surface of the water layer and, unlike for smaller clusters, equilibrium "encapsulated" structures where the N_2O_5 molecule is surrounded by several water molecules. These two categories are potentially important because they may help us understand N_2O_5 entry from the surface into the bulk. Considering C_2 and C_s initial symmetries for N_2O_5, we find four $N_2O_5 \cdot (H_2O)_{20}$ structures, two "surface" and two "encapsulated", presented in Figure 9. Relative energies, bond lengths and values of the angles and dihedral angles are also shown. Panels (a) and (b), correspond to optimized structures with C_2 initial structure for N_2O_5. Comparing the distortion of the "surface" N_2O_5 structure (a) with the n = 10 and n = 15 clusters shown in the previous subsection, we see a more pronounced change in the dihedral angles (1° and 8°), with N_2O_5 being almost completely planar. The solvation effects on the "encapsulated" structure (b) are very interesting; one central N-O bond is more elongated than for smaller "surface" clusters, to a value of 1.99 Å. We show in the following subsections that the N_2O_5 in this structure has a significant charge separation and binding energy that nearly correspond to a contact ion pair.

Panels (c) and (d) of Figure 9 present structures optimized from an initial C_s N_2O_5 geometry. The “surface” structure (c) is the most stable of the four local minima identified while the “encapsulated” structure (d) is 7.8 kcal mol^{-1} higher in energy. For the (c) and (d) structures, the 20 water molecules do not distort the dihedral angles as much as for n = 10 and n = 15. However, the effect of increased solvation is seen on the elongation of longer central N-O bond, where a clear trend in bond length emerges: 1.54 Å (n = 10) < 1.59 Å (n = 15) < 1.69 Å (n = 20 “surface”) < 1.71 Å (n = 20 “encapsulated”).

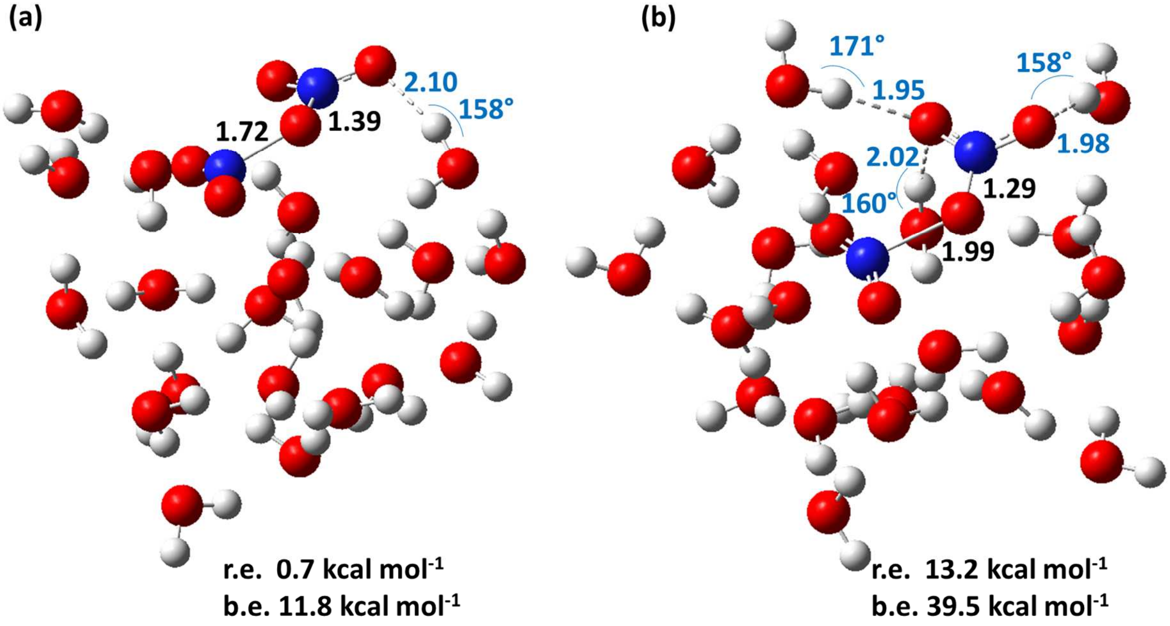

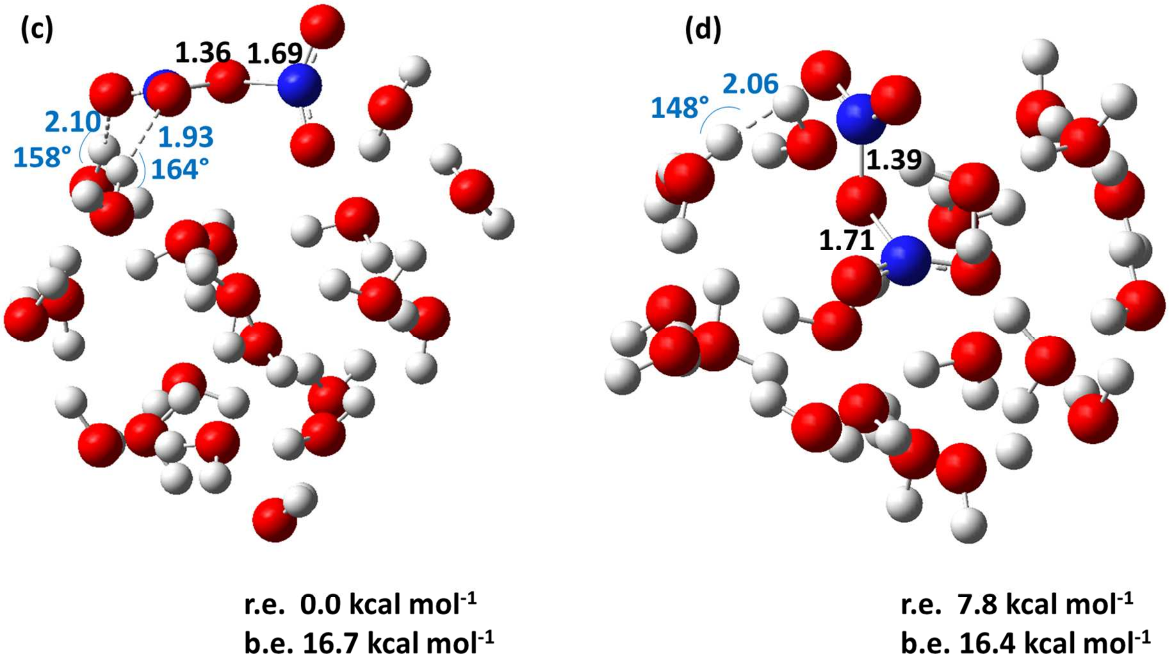

Figure 9. $N_2O_5{\cdot}(H_2O)_{20}$ clusters, with N_2O_5 on the surface and "encapsulated". **(a)** C_2 "surface", **(b)** C_2 "encapsulated", **(c)** C_s "surface", and **(d)** C_s "encapsulated". Relative energies (r.e.), compared to lowest energy structure for each size, and binding energies (b.e.) are given below each structure. Bond lengths of the central N-O bonds are given in black and hydrogen-acceptor distances and hydrogen bond angles are given in blue.

(b) Charge separation

McNamara and Hillier[34] state that the increased solvation by water molecules produces a strong polarization and distorts the N_2O_5 geometry, forming solvated NO_2^+. This is believed to favor the hydrolysis of N_2O_5 into HNO_3, due to an increased electrophilicity of one of the N atoms. However, this mechanism is still under debate.[28] Thus, it is useful to investigate the role of increasing number of water molecules and their role as a polar medium in stabilizing charge separation.

The partial charge on each atom was calculated by NBO. To calculate the total charge on $NO_2^{\delta+}$ and $NO_3^{\delta-}$, we adopted the criterion that the central O atom and the NO_2 group to which the distance is shorter after optimization is contained in $NO_3^{\delta-}$. In Figure 10 we plot the partial charge on the $NO_2^{\delta+}$ group in panel (a), and the distance of the longer N-O bond in panel (b) as a function of number of water molecules in the cluster. The partial charge on $NO_3^{\delta-}$ mirrors the charge on $NO_2^{\delta+}$. From the data we see a clear trend: the longer the N-O bond, the higher the charge separation. Concerning the charge separation as a function of the number of water molecules, the analysis is not so straightforward. We do not observe a systematic rise in charge separation when *n* increases in the series 1-4, 6, 10, 15, and 20. Most charges obtained in this section are within the range of dynamical fluctuations observed in the scattering simulations of Section II. However, the most interesting feature in Figure 10 is seen for the "encapsulated" $N_2O_5(H_2O)_{20}$ cluster, which is based on the initial C_2 structure. One N-O bond is significantly stretched to 1.99 Å and the corresponding partial charges are ±0.6 a.u. This indicates that the structure formed is a contact ion-pair. The charge separation is analyzed further in the next subsection in the context of contributions to the binding energy.

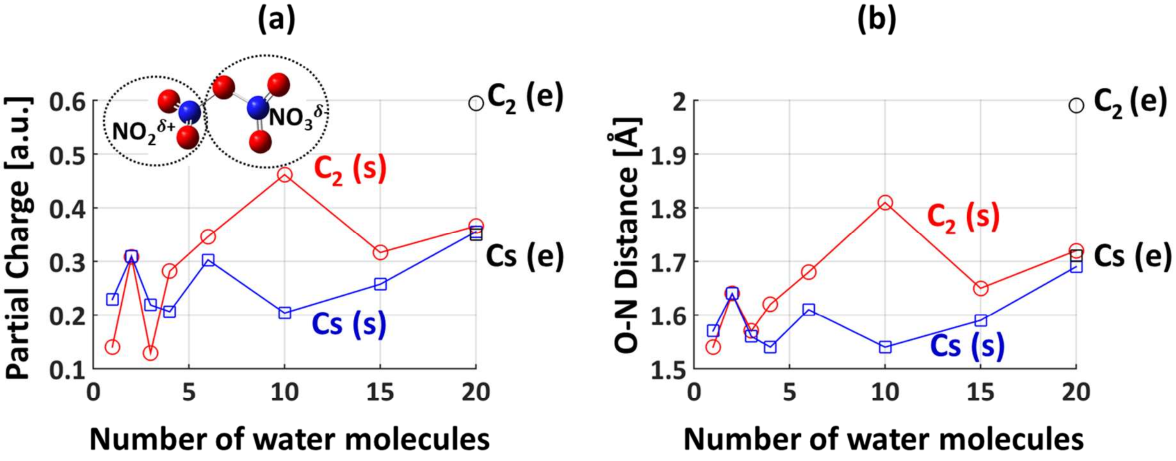

Figure 10. (a) NBO partial charges for $NO_2^{\delta+}$, and (b) The longer central N-O bond distance in Å, as a function of number of water molecules for $N_2O_5{\cdot}H_2O_{(n)}$ with *n* = 1-4, 6, 10, 15, and 20. In red: values corresponding to the "C_2" clusters series; in black: values corresponding to the "C_s" clusters series. "(s)" marks "surface" clusters and for *n*

= 20, “(e)” marks “encapsulated” clusters. Partial charges on $NO_3^{\delta-}$ are not shown but simply mirror the $NO_2^{\delta+}$ partial charges.

(c) Binding forces: contributions from hydrogen bonding and multipolar interactions

The strength of the interactions between N_2O_5 and the water molecules in each cluster can be quantified by calculating the binding energy of the system. The binding energies for the 18 amorphous clusters studied here range from 4.3 to 39.5 kcal mol^{-1} (see Figures 6, 7 and 9 above and the SI). In addition, using the same geometrical criteria for hydrogen bonds described in Section II, we find that in most cases N_2O_5 forms zero to one hydrogen bonds with water, in accordance with the scattering simulations. Only in a few cases can we identify two hydrogen bonds, and the largest value found is three hydrogen bonds for the cluster of $n = 10$ (C_2) and for the “encapsulated” $n = 20$ (C_2) cluster. The hydrogen-acceptor distances in Å and corresponding D-H···A angles in degrees are given in blue in all the figures in this section as well as in the SI for the structures not shown here.

The energy of a weak hydrogen bond, according to the definition of Hibbert and Emsley, ranges between 2.4 to 12 kcal mol^{-1}. [82] For the clusters presented here, we estimated the hydrogen bond energies, using the quantum theory of atoms in molecules (QTAIM)[83,84] and the Espinosa method,[85] to be ≤ 5 kcal mol^{-1} (full details are given in the SI). This is reasonable, due to the significant deviations from linearity and long donor-acceptor distances. Considering the values of the total binding energies and the small number of weak hydrogen bonds that are formed in most local minima structures considered, we conclude that hydrogen bonds alone do not account for the total binding energy. The other contribution to the total binding energy is due to multipolar interactions. By multipolar interactions, we mean interactions between partial charges on N_2O_5 and on water. As discussed previously, the water molecules distort the N_2O_5 geometry and cause a charge separation in the molecule. Consistent with this analysis, for smaller clusters (n = 1-6) where water generally distorts N_2O_5 to a lesser extent than in the bigger clusters (n = 10, 15, 20), the binding energy is smaller. For the $N_2O_5\cdot(H_2O)_{20}$ "encapsulated" C_2 cluster, which has the largest charge on the $NO_2^{\delta+}$ fragment (0.6 a.u.), the binding energy is also the largest of all clusters, being 40 kcal mol^{-1}. This large charge separation also strongly suggests that the structure is in fact a contact ion-pair. The formation of an ion-pair structure is consistent with the fact that it also has the largest number of hydrogen bonds, of all structures considered here, which are formed due to the solvation of the $NO_3^{\delta-}$ fragment.

From the results presented and analyzed in this section, we conclude that increasing the number of water molecules in a cluster induces charge separation of N_2O_5 into $NO_2^{\delta+}$ and $NO_3^{\delta-}$; this effect becomes dramatic for N_2O_5 in the bulk of a 20 water-molecule cluster. The water molecules induce geometrical distortions of N_2O_5 and stabilize the partial charges generated by those distortions.

IV. Thermodynamics of N_2O_5 adsorption and solvation at the water/vapor interface

As mentioned in the introduction, the solubility of N_2O_5 in bulk water is an important ingredient in atmospheric models of N_2O_5 reactivity.[21] However, only estimates are available at present[49] because N_2O_5 hydrolyzes rapidly in water and no experimental measurements have been able to capture its physical solubility. In this section we investigate the process of aqueous solvation of N_2O_5 by means of classical MD simulations with an empirical potential. We evaluate the free energy profile, or potential of mean force (PMF), associated with transporting N_2O_5 from the gas phase across the water/vapor interface into the aqueous bulk, which provides an estimate of the solubility of N_2O_5. The simulations also provide insight into hydrogen bonding during the process of solvation.

(a) Model system and computational methods

The MD simulations were performed with the sander program of the AmberTools software package[86,87] employing periodic boundary conditions in the canonical (NVT) ensemble. A real-space cutoff of 9.0 Å was applied to non-bonded interactions and the particle mesh Ewald summation method[88] was used to treat all long-range electrostatics. A time step of 2 fs was used and bonds involving hydrogen atoms were constrained using the SHAKE algorithm[89] with a relative tolerance of 10^{-6}. The temperature was kept at 300 K using Langevin dynamics[90] with a collision frequency of 5.0 ps^{-1}. MD trajectories were analyzed with the cpptraj program.[91]

Our model of liquid water consists of 1024 water molecules that were placed inside a rectangular simulation box of 90.0 x 30.0 x 30.0 $Å^3$, thus forming a slab of liquid with two water/vapor interfaces. The x-axis coincides with the direction normal to the water/vapor interfaces. A single N_2O_5 molecule was introduced into the gas phase above the water/vapor interface. The TIP4P/2005 force field[92] was used for water, which provides a good description of the water phase diagram over a wide range of temperatures and pressures.[93,94] For N_2O_5 we employed parameters from the general Amber force field (GAFF)[95] in combination with AM1-BCC charges,[96] which are appropriate for use in condensed-phase simulations. This force field is non-polarizable and hence does not explicitly account for electronic polarization and the charge fluctuations that were discussed in previous sections. However, polarization effects are implicitly taken into account in an average fashion by means of parameterization of the TIP4P/2005 water model and the atomic partial charges from the AM1-BCC model, which are increased relative to gas phase values, thus accounting for the average polarization effect of the aqueous environment. The charges on the NO_3^- and NO_2^+ fragments are ±0.186, which compares well to the average charge distribution at the water surface and in bulk water that we observed in our DFT-based MD simulations in section II (see Figure 3).

The simulation setup is shown in Figure 11. We used the PLUMED plugin[97] to apply a harmonic constraint (biasing potential) along the x-component of the distance between the center of mass (COM) of the N_2O_5 molecule and the COM of the water molecules with a force constant of 5.0 kcal mol^{-1}. This potential constrains the distance between N_2O_5 and the water surface but does not impose any restriction on the motion of either water or solute molecules in the xy-plane. The system was equilibrated for 10 ns with a COM distance constraint of 36 Å, which corresponds to a distance of N_2O_5 of approximately 19 Å from the water surface. The water density profile is plotted in Figure 11 along with the Gibbs dividing surfaces (GDS) of the two water/vapor interfaces (dashed vertical lines), where the density is half of the bulk density. The equilibrated system has a water density of 0.981 g/cm^3 at the center of the slab and a slab thickness of 34.6 Å, measured as the distance between the upper and lower GDS.

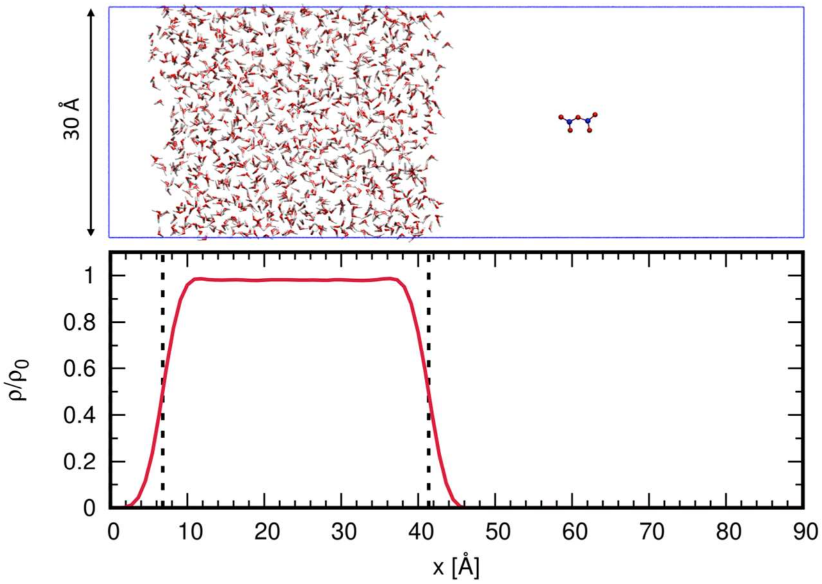

Figure 11. (top) Model for free energy calculations of N_2O_5 solvation in a slab of liquid water. (bottom) Water density (red solid line) and position of Gibbs dividing surfaces (black dashed vertical lines).

The free energy profile for the transfer of N_2O_5 from the gas phase to the bulk liquid was computed from a set of umbrella sampling simulations that utilized the x-component of the COM distance as collective variable. We pulled the N_2O_5 molecule slowly along the x-coordinate across the water/vapor interface to the center of the water slab by adjusting the COM restraint over a period of 1.44 ns. Thus, pulling was carried out sufficiently slowly for the system not to depart significantly from equilibrium. At intervals of 0.5 Å we extracted configurations and performed constraint MD simulations of 6 ns length. We discarded the first ns of each window, thus monitoring the collective variable for a total of 5 ns MD simulation for each of the 91 windows. The free energy profile was obtained from this data by umbrella integration,[98] that is integration of the mean force with respect to the collective variable. By computing the free energy profile separately over the first and last 2.5 ns of simulation, we estimate the statistical sampling error of the calculated free energy values to be approximately ± 0.1 kcal mol^{-1} by taking the difference between the corresponding two values of free energy.

The free energy thus obtained is a Helmholtz free energy, because the simulations are performed in the canonical ensemble. However, the simulation conditions actually resemble the isothermal-isobaric (NPT) ensemble because the open water/vapor interfaces allow the volume of the water slab to fluctuate. Thus, the calculated free energy is comparable to the experimentally accessible Gibbs free energy *G*.

(b) Free energy profile

The calculated free energy profile for the transfer of N_2O_5 from the gas phase across the water/vapor interface into bulk water is shown in Figure 12. The free energy is defined up to an arbitrary constant and we have chosen the free energy of N_2O_5 in gas phase as zero. As the molecule moves from the gas phase towards the bulk liquid water, the free energy goes through a minimum at the water surface, then increases, surmounts a small barrier of 1.8 kcal mol^{-}

[1], and reaches a plateau in the interior of the water slab. Similar free energy profiles have also been observed in simulations of other atmospherically relevant gases.[44,45,99] The free energy difference ΔG_{12} between two points along the path corresponds to a molecular concentration ratio of the solute at these points,

$$\frac{c_1}{c_2} = \exp(-\Delta G_{12}/RT)$$

where R is the gas constant and T is the temperature. The free energy minimum at the surface of the water slab therefore gives rise to a significant concentration enhancement of N_2O_5 in the interfacial region with respect to both the bulk liquid phase and the gas phase concentrations. This surface concentration enhancement and the barriers to bulk solvation and desorption are consistent with the surface trapping that we observed in the AIMD simulations of N_2O_5 scattering in section II, in which we observed sticking of N_2O_5 to the surface.

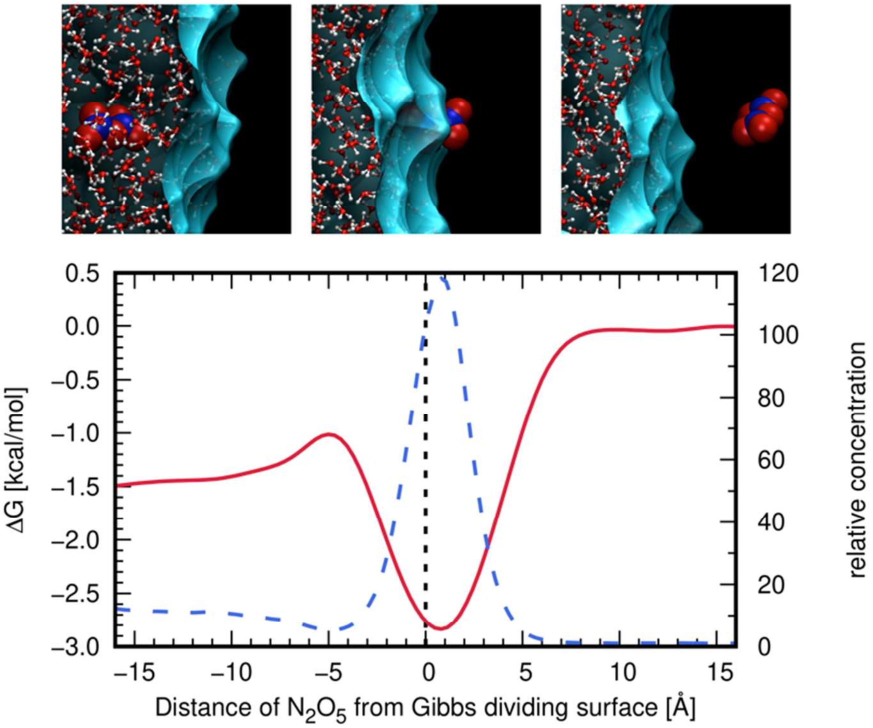

Figure 12. Free energy profile (red solid curve) and the corresponding concentration profile (blue dashed curve) for transfer of N_2O_5 from the gas phase (to the right of the

Gibbs dividing surface) across the water/vapor interface into bulk water (to the left of the Gibbs dividing surface) obtained from classical MD simulations with TIP4P/2005 and GAFF. Snapshots from simulations along the reaction coordinate with a rendering of the instantaneous water surface are shown above the plot.

The solvation free energy ΔG_{solv} is the free energy difference between the gas phase and the bulk liquid phase. It determines the physical solubility of a gas and can be related to Henry's law constant k_{H}, which is usually expressed as the concentration of a molecule in the liquid divided by its partial pressure in the gas phase,[50]

$$k_{\mathrm{H}}^{\mathrm{cp}} = \frac{c_{\mathrm{l}}}{p_{\mathrm{g}}}$$

Henry's law can also be written in dimensionless form using the concentrations in the liquid and gas phases,

$$k_{\mathrm{H}}^{\mathrm{cc}} = \frac{c_{\mathrm{l}}}{c_{\mathrm{g}}}$$

These constants are related to the solvation free energy of a single gas molecule at infinite dilution that is obtained from our MD simulations via the following equation,

$$k_{\mathrm{H}}^{\mathrm{cc}} = k_{\mathrm{H}}^{\mathrm{cp}} RT = \exp(-\Delta G_{\mathrm{solv}}/RT)$$

The solvation free energy of N_2O_5 from our MD simulations is –1.5 kcal mol^{-1}, which corresponds to a Henry's law solubility of $k_{\mathrm{H}}^{\mathrm{cp}} = 0.5\ \mathrm{M/atm}$. This value corresponds to the physical solubility of N_2O_5 (before hydrolysis) and falls just below the 1 to 10 M atm range estimated previously.[49–51,100]

Finally, we would like to note that while the general shape of the free energy profile is likely correct, the solvation free energy is rather sensitive to the quality of the force field that is employed in the MD simulations. In order to make truly quantitative predictions about the solubility of N_2O_5, it will be necessary to employ a potential energy function that explicitly includes polarization as well as captures short-range quantum-mechanical many-body effects such as the highly successful MB-pol,[101,102] which is the only water model that was shown to accurately reproduce the properties of water from small clusters up to the condensed phase.[103] Work along these lines is on the way.

(c) Hydrogen bonding

Figure 13 shows a depth profile of the probability of hydrogen bond formation between N_2O_5 and water molecules, employing the same geometric definition of a hydrogen bond as in section II. As the molecule approaches the surface hydrogen bonds start to form and the probability to form hydrogen bonds is slightly higher in bulk than at the water/vapor interface. In agreement with the AIMD simulations from section II, we find the probability of hydrogen bond formation to be very low. Even when solvated in bulk water, N_2O_5 is most likely not to form any hydrogen bond to water (probability of 76%). The probability to form a single hydrogen bond is 23% and the probability to form two or more hydrogen bonds to water molecules at the same time is close to zero. This indicates that N_2O_5 is not well solvated by water, which is of course also reflected in the small solvation free energy and the corresponding low solubility.

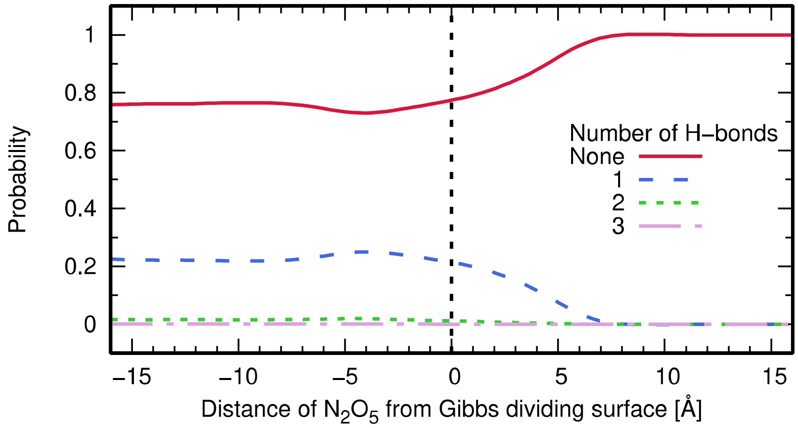

Figure 13. Probability of hydrogen bond formation between N_2O_5 and water obtained from classical MD simulations with TIP4P/2005 and GAFF.

V. Summary and Atmospheric Implications

This paper presents a comprehensive theoretical study of the interactions between N_2O_5 and water media. The main conclusions drawn from the results presented here are: 1) N_2O_5 is trapped at the surface of pure liquid water, upon impact from the gas-phase. This was shown through MD simulations of the scattering process in which N_2O_5 remained trapped for 20-25 ps after collision. It was also corroborated by a calculation of the PMF to transfer an intact N_2O_5 molecule from the gas-phase, through the interface and into the bulk, which showed a minimum in the free-energy at the surface of water. 2) Water molecules induce a charge separation within the N_2O_5 molecule which is on the order of ~0.2 a.u. This was shown both for N_2O_5 trapped at the air/water interface, in bulk water and through calculations done on water clusters of nanometric sizes. For the largest water cluster studied, with 20 water molecules, a single structure of N_2O_5 in a more solvated environment showed a much larger charge separation, of approximately 0.6 a.u. 3) N_2O_5 is very weakly solvated by the water environment, forming almost no hydrogen bonds, both at the interface, in bulk water and in nanometric clusters.

Laboratory measurements and field observations have shown that the reactive uptake of N_2O_5 to atmospheric aerosol particles spans at least four orders of magnitude.[4,104,105] Current parameterizations of N_2O_5 reactive uptake, that can be implemented in regional scale air quality models,[106] fail to capture the observed variability in N_2O_5 reactivity.[107] The inability of existing models to adequately capture N_2O_5 reaction chemistry is in part due to the absence of accurate constraints on the reaction mechanism, the individual reaction rates, the role of interfacial ions in the initial dissociation of N_2O_5, the entry probability of N_2O_5 through complex organic surfactants, and even the physical solubility of N_2O_5 in water. As a result, the rate of N_2O_5 reactive uptake that is derived from these parameterizations is largely empirical, making extension of laboratory measurements to more chemically complex surfaces prohibitive. Even with accurate input constraints, it is not clear whether steady-state models, such as the resistor model, can be used to capture the reactive uptake of sparingly soluble, yet highly reactive molecules such as N_2O_5.

While it is most likely that organic constituents in atmospheric aerosol play a heavy hand in driving the observed variance in N_2O_5 reactivity, we stress that a molecular foundation for how N_2O_5 reacts even with pure water has been elusive. In this manuscript, we have provided a unique theoretical perspective on both the dynamic first 20-25 ps following the collision of N_2O_5 with pure water and a thermodynamic equilibrium perspective for the free energy profile of an intact N_2O_5 travelling from the gas-phase across the vapor/water interface into the bulk. The calculations described here do not yet provide the needed constraints for atmospheric models, but they offer a molecular foundation for N_2O_5 reactions at aqueous interfaces and a pathway toward accurate determinations of key elements of the N_2O_5 reaction.

Acknowledgements

This work was funded by the National Science Foundation through the Center for Aerosol Impacts on Chemistry of the Environment under grant no. CHE-1305427. B.H. was supported through an Adams fellowship of the Israel Academy of Sciences and Humanities and through the Rahamimoff travel grant for young scientists of the United States - Israel Binational Science Foundation (BSF). This work used the Extreme Science and Engineering Discovery Environment (XSEDE), which is supported by National Science Foundation grant number ACI-1548562.[58] B.H. thanks G. Murdachaew, D. Harries and C. Allolio for valuable discussions regarding the MD simulations. A.W.G. acknowledges helpful discussions with Francesco Paesani and Sandeep Reddy regarding the classical MD simulations.

References

1 Barbara J. Finlayson-Pitts and James N. Pitts, *Chemistry of the Upper and Lower Atmosphere*, Academic Press, San Diego, 2000.

2 J. H. Seinfeld and S. N. Pandis, *Atmospheric Chemistry and Physics: From Air Pollution to Climate Change*, Wiley-VCH, New York, 1997.

3 P. J. Crutzen, *Ann. Rev. Earth Planet. Sci.*, 1979, **7**, 443–72.

4 W. L. Chang, P. V. Bhave, S. S. Brown, N. Riemer, J. Stutz and D. Dabdub, *Aerosol Sci. Technol.*, 2011, **45**, 655–685.

5 H. D. Osthoff, R. Sommariva, T. Baynard, A. Pettersson, E. J. Williams, B. M. Lerner, J. M. Roberts, H. Stark, P. D. Goldan, W. C. Kuster, T. S. Bates, D. J. Coffman, A. R. Ravishankara and S. S. Brown, *J. Geophys. Res. Atmos.*, 2006, **111**, 1–13.

6 S. S. Brown and J. Stutz, *Chem. Soc. Rev.*, 2012, **41**, 6405–6447.

7 F. J. Dentener and P. J. Crutzen, *J. Geophys. Res. Atmos.*, 1993, **98**, 7149–7163.

8 M. J. Evans and D. J. Jacob, *Geophys. Res. Lett.*, 2005, **32**, 1–4.

9 H. L. MacIntyre and M. J. Evans, *Atmos. Chem. Phys.*, 2010, **10**, 7409–7414.

10 V. Vaida, *J. Chem. Phys.*, 2011, **135**, 20901.

11 N. Riemer, *J. Geophys. Res.*, 2003, **108**, 4144.

12 U. F. Platt, A. M. Winer, H. W. Biermann, R. Atkinson and J. N. Pitts, *Environ. Sci. Technol.*, 1984, **18**, 365–369.

13 S. S. Brown, J. E. Dibb, H. Stark, M. Aldener, M. Vozella, S. Whitlow, E. J. Williams, B. M. Lerner, R. Jakoubek, A. M. Middlebrook, J. A. DeGouw, C. Warneke, P. D. Goldan, W. C. Kuster, W. M. Angevine, D. T. Sueper, P. K. Quinn, T. S. Bates, J. F. Meagher, F. C. Fehsenfeld and A. R. Ravishankara, *Geophys. Res. Lett.*, 2004, **31**, 2–6.

14 M. Mozurkewich and J. G. Calvert, *J. Geophys. Res. Atmos.*, 1988, **93**, 15889–15896.

15 J. A. Thornton and J. P. D. Abbatt, *J. Phys. Chem. A*, 2005, **109**, 10004–10012.

16 B. J. Finlayson-Pitts, M. J. Ezell and J. N. Pitts Jr., *Nature*, 1989, 337, 241–244.

17 R. C. Hoffman, M. E. Gebel, B. S. Fox and B. J. Finlayson-Pitts, *Phys. Chem. Chem. Phys.*, 2003, **5**, 1780–1789.

18 J. A. Thornton, J. P. Kercher, T. P. Riedel, N. L. Wagner, J. Cozic, J. S. Holloway, W. P. Dubé, G. M. Wolfe, P. K. Quinn, A. M. Middlebrook, B. Alexander and S. S. Brown, *Nature*, 2010, **464**, 271–274.

19 A. D. Hammerich, B. J. Finlayson-Pitts and R. B. Gerber, *Phys. Chem. Chem. Phys.*, 2015, **17**, 19360–19370.

20 U. Pöschl, *Angew. Chemie Int. Ed.*, 2005, **44**, 7520–7540.

21 J. P. D. Abbatt, A. K. Y. Lee and J. A. Thornton, *Chem. Soc. Rev.*, 2012, **41**, 6555–6581.

22 E. E. McDuffie, D. L. Fibiger, W. P. Dubé, F. Lopez-Hilfiker, B. H. Lee, J. A. Thornton, V. Shah, L. Jaeglé, H. Guo, R. J. Weber, J. Michael Reeves, A. J. Weinheimer, J. C. Schroder, P. Campuzano-Jost, J. L. Jimenez, J. E. Dibb, P. Veres, C. Ebben, T. L. Sparks, P. J. Wooldridge, R. C. Cohen, R. S. Hornbrook, E. C. Apel, T. Campos, S. R. Hall, K. Ullmann and S. S. Brown, *J. Geophys. Res. Atmos.*, 2018, 1–28.

23 G. Luo and X. Chen, *J. Phys. Chem. Lett.*, 2012, **3**, 1147–1153.

24 A. Stirling, I. Pápai, J. Mink and D. R. Salahub, *J. Chem. Phys.*, 1994, **100**, 2910–2923.

25 L. C. Jitariu and D. M. Hirst, *Phys. Chem. Chem. Phys.*, 2000, **2**, 847–852.

26 J. □U. Grabow, A. M. Andrews, G. T. Fraser, K. K. Irikura, R. D. Suenram, F. J. Lovas, W. J. Lafferty and J. L. Domenech, *J. Chem. Phys.*, 1996, **105**, 7249–7262.

27 J. A. Snyder, D. Hanway, J. Mendez, A. J. Jamka and F.-M. Tao, *J. Phys. Chem. A*, 1999, **103**, 9355–9358.

28 R. Bianco and J. T. Hynes, *Int. J. Quantum Chem.*, 1999, **75**, 683–692.

29 A. F. Voegele, C. S. Tautermann, T. Loerting and K. R. Liedl, *Phys. Chem. Chem. Phys.*, 2003, **5**, 487–495.

30 D. Hanway and F.-M. Tao, *Chem. Phys. Lett.*, 1998, **285**, 459–466.

31 J. D. Raff, B. Njegic, W. L. Chang, M. S. Gordon, D. Dabdub, R. B. Gerber and B. J. Finlayson-Pitts, *Proc. Natl. Acad. Sci.*, 2009, **106**, 13647–13654.

32 J. P. McNamara and I. H. Hillier, *Phys. Chem. Chem. Phys.*, 2000, **2**, 2503–2509.

33 I. M. Alecu and P. Marshall, *J. Phys. Chem. A*, 2014, **118**, 11405–11416.

34 J. P. McNamara and I. H. Hillier, *J. Phys. Chem. A*, 2000, **104**, 5307–5319.

35 P. J. Kelleher, F. S. Menges, J. W. DePalma, J. K. Denton, M. A. Johnson, G. H. Weddle, B. Hirshberg and R. B. Gerber, *J. Phys. Chem. Lett.*, 2017, 4710–4715.

36 C. J. Gaston and J. A. Thornton, *J. Phys. Chem. A*, 2016, **120**, 1039–1045.

37 G. Murdachaew, M. E. Varner, L. F. Phillips, B. J. Finlayson-Pitts and R. B. Gerber, *Phys. Chem. Chem. Phys.*, 2013, **15**, 204–212.

38 R. B. Gerber, M. E. Varner, A. D. Hammerich, S. Riikonen, G. Murdachaew, D. Shemesh and B. J. Finlayson-Pitts, *Acc. Chem. Res.*, 2015, **48**, 399–406.

39 L. Partanen, G. Murdachaew, R. B. Gerber and L. Halonen, *Phys. Chem. Chem. Phys.*, 2016, **18**, 13432–13442.

40 G. Murdachaew, G. M. Nathanson, R. Benny Gerber and L. Halonen, *Phys. Chem. Chem. Phys.*, 2016, **18**, 29756–29770.

41 T. Lewis, B. Winter, A. C. Stern, M. D. Baer, C. J. Mundy, D. J. Tobias and J. C. Hemminger, *J. Phys. Chem. C*, 2011, **115**, 21183–21190.

42 M. D. Baer, D. J. Tobias and C. J. Mundy, *J. Phys. Chem. C*, 2014, **118**, 29412–29420.

43 B. Hirshberg and R. B. Gerber, *J. Phys. Chem. Lett.*, 2016, **7**, 2905–2909.

44 R. Vácha, P. Slavíček, M. Mucha, B. J. Finlayson-Pitts and P. Jungwirth, *J. Phys. Chem. A*, 2004, **108**, 11573–11579.

45 J. Vieceli, M. Roeselova, N. Potter, L. X. Dang, B. C. Garrett and D. J. Tobias, *J. Phys. Chem. B*, 2005, **109**, 15876–15892.

46 L. S. E. Romero Lejonthun, P. U. Andersson, M. Hallquist, E. S. Thomson and J. B. C. Pettersson, *J. Phys. Chem. B*, 2014, **118**, 13427–13434.

47 M. A. Shaloski, J. R. Gord, S. Staudt, S. L. Quinn, T. H. Bertram and G. M. Nathanson, *J. Phys. Chem. A*, 2017, **121**, 3708–3719.

48 R. A. Relph, T. L. Guasco, B. M. Elliott, M. Z. Kamrath, A. B. McCoy, R. P. Steele, D. P. Schofield, K. D. Jordan, A. A. Viggiano, E. E. Ferguson and M. A. Johnson, *Science (80-.).*, 2010, **327**, 308–312.

49 A. Fried, B. E. Henry, J. G. Calvert and M. Mozurkewich, *J. Geophys. Res.*, 1994, **99**, 3517–3532.

50 R. Sander, *Atmos. Chem. Phys.*, 2015, **15**, 4399–4981.

51 T. F. Mentel, M. Sohn and A. Wahner, *Phys. Chem. Chem. Phys.*, 1999, **1**, 5451–5457.

52 A. Tabazadeh and R. P. Turco, *J. Geophys. Res.*, 1993, **98**, 12727.

53 A. D. Hammerich, B. J. Finlayson-Pitts and R. B. Gerber, *J. Phys. Chem. Lett.*,

2012, **3**, 3405–3410.

54 G. J. Martyna, M. L. Klein and M. Tuckerman, *J. Chem. Phys.*, 1992, **97**, 2635–2643.

55 S. Pronk, S. Páll, R. Schulz, P. Larsson, P. Bjelkmar, R. Apostolov, M. R. Shirts, J. C. Smith, P. M. Kasson, D. van der Spoel, B. Hess and E. Lindahl, *Bioinformatics*, 2013, **29**, 845–854.

56 J. Vandevondele, M. Krack, F. Mohamed, M. Parrinello, T. Chassaing and J. Hutter, *Comput. Phys. Commun.*, 2005, **167**, 103–128.

57 J. Hutter, M. Iannuzzi, F. Schiffmann and J. Vandevondele, *Wiley Interdiscip. Rev. Comput. Mol. Sci.*, 2014, **4**, 15–25.

58 J. Towns, T. Cockerill, M. Dahan, I. Foster, K. Gaither, A. Grimshaw, V. Hazlewood, S. Lathrop, D. Lifka, G. D. Peterson, R. Roskies, J. R. Scott and N. Wilkens-Diehr, *Comput. Sci. Eng.*, 2014, **16**, 62–74.

59 J. Perdew, K. Burke and M. Ernzerhof, *Phys. Rev. Lett.*, 1996, **77**, 3865–3868.

60 S. Grimme, J. Antony, S. Ehrlich and H. Krieg, *J. Chem. Phys.*, 2010, **132**, 154104.

61 S. Grimme, S. Ehrlich and L. Goerigk, *J. Comput. Chem.*, 2011, **32**, 1456–1465.

62 J. VandeVondele and J. Hutter, *J. Chem. Phys.*, 2007, **127**, 114105.

63 S. Goedecker, M. Teter and J. Hutter, *Phys. Rev. B*, 1996, **54**, 1703–1710.

64 G. J. Martyna and M. E. Tuckerman, *J. Chem. Phys.*, 1999, **110**, 2810–2821.

65 A. Barducci, G. Bussi and M. Parrinello, *Phys. Rev. Lett.*, 2008, **100**, 1–4.

66 T. H. Bertram, J. A. Thornton and T. P. Riedel, *Atmos. Meas. Tech.*, 2009, **2**, 231–242.

67 W. Humphrey, A. Dalke and K. Schulten, *J. Mol. Graph.*, 1996, **14**, 33–38.

68 B. W. McClelland, L. Hedberg, K. Hedberg and K. Hagen, *J. Am. Chem. Soc.*, 1983, **105**, 3789–3793.

69 B. M. McClelland, A. D. Richardson and K. Hedberg, *Helv. Chim. Acta*, 2001, **84**, 1612–1624.

70 J.-D. Chai and M. Head-Gordon, *Phys. Chem. Chem. Phys.*, 2008, **10**, 6615–6620.

71 T. H. Dunning, *J. Chem. Phys.*, 1989, **90**, 1007–1023.

72 A. Becke, *J. Chem. Phys.*, 1993, **98**, 5648–5652.

73 P. J. Stephens, F. J. Devlin, C. F. Chabalowski and M. J. Frisch, *J. Phys. Chem.*, 1994, **98**, 11623–11627.

74 C. T. Wolke, J. A. Fournier, E. Miliordos, S. M. Kathmann, S. S. Xantheas and M. A. Johnson, *J. Chem. Phys.*, 2016, **144**, 74305.

75 J. A. Fournier, C. T. Wolke, M. A. Johnson, T. T. Odbadrakh, K. D. Jordan, S. M. Kathmann and S. S. Xantheas, *J. Phys. Chem. A*, 2015, **119**, 9425–9440.

76 N. Heine, M. R. Fagiani and K. R. Asmis, *J. Phys. Chem. Lett.*, 2015, **6**, 2298–2304.

77 M. R. Fagiani, H. Knorke, T. K. Esser, N. Heine, C. T. Wolke, S. Gewinner, W. Schöllkopf, M.-P. Gaigeot, R. Spezia, M. A. Johnson and K. R. Asmis, *Phys. Chem. Chem. Phys.*, 2016, **18**, 26743–26754.

78 L. Martinez, R. Andrade, E. G. Birgin and J. M. Martínez, *J. Comput. Chem.*, 2009, **30**, 2157–2164.

79 M. J. Frisch, G. W. Trucks, H. B. Schlegel, G. E. Scuseria, M. A. Robb, J. R. Cheeseman, G. Scalmani, V. Barone, G. A. Petersson, H. Nakatsuji, X. Li, M. Caricato, A. Marenich, J. Bloino, B. G. Janesko, R. Gomperts, B. Mennucci, H. P. Hratchian, J. V. Ortiz, A. F. Izmaylov, J. L. Sonnenberg, D. Williams-Young, F. Ding, F. Lipparini, F. Egidi, J. Goings, B. Peng, A. Petrone, T. Henderson, D. Ranasinghe, V. G. Zakrzewski, J. Gao, N. Rega, G. Zheng, W. Liang, M. Hada, M. Ehara, K. Toyota, R. Fukuda, J. Hasegawa, M. Ishida, T. Nakajima, Y. Honda, O. Kitao, H. Nakai, T. Vreven, K. Throssell, J. A. Montgomery, J. E. Peralta, F. Ogliaro, M. Bearpark, J. J. Heyd, E. Brothers, K. N. Kudin, V. N. Staroverov, T. Keith, R. Kobayashi, J. Normand, K. Raghavachari, A. Rendell, J. C. Burant, S. S. Iyengar, J. Tomasi, M. Cossi, J. M. Millam, M. Klene, C. Adamo, R. Cammi, J. W. Ochterski, R. L. Martin, K. Morokuma, O. Farkas, J. B. Foresman and D. J. Fox, *Gaussian 09, Revis. D.01*, 2009.

80 A. E. Reed, L. A. Curtiss and F. Weinhold, *Chem. Rev.*, 1988, **88**, 899–926.

81 F. B. van Duijneveldt, J. G. C. M. van Duijneveldt-van de Rijdt and J. H. van Lenthe, *Chem. Rev.*, 1994, **94**, 1873–1885.

82 F. Hibbert and J. Emsley, *Adv. Phys. Org. Chem.*, 1990, **26**, 255–379.

83 R. F. W. Bader, *Chem. Rev.*, 1991, **91**, 893–928.

84 R. F. W. Bader, *Acc. Chem. Res.*, 1985, **18**, 9–15.

85 E. Espinosa, E. Molins and C. Lecomte, *Chem. Phys. Lett.*, 1998, **285**, 170–173.

86 D. A. Case, D. S. Cerutti, T. E. C. III, T. A. Darden, R. E. Duke, T. J. Giese, H. Gohlke, A. W. Goetz, D. Greene, N. Homeyer, S. Izadi, A. Kovalenko, T. S. Lee, S. LeGrand, P. Li, C. Lin, J. Liu, T. Luchko, R. Luo, A. D. Mermelstein, K.M. Merz, G. Monard, H. Nguyen, I. Omelyan, A. Onufriev, F. Pan, R. Qi, D.R. Roe, X. Roitberg, C. Sagui, C.L. Simmerling, W.M. Botello-Smith, J. Swails, R.C. Walker, J. Wang, R.M. Wolf, D. M. Y. Wu, L. Xiao and P. A. Kollman, *AMBER2017*, University of California, San Francisco, 2017.

87 R. Salomon-Ferrer, D. A. Case and R. C. Walker, *Wiley Interdiscip. Rev. Comput. Mol. Sci.*, 2013, **3**, 198–210.

88 T. Darden, D. York and L. Pedersen, *J. Chem. Phys.*, 1993, **98**, 10089–10092.

89 S. Miyamoto and P. A. Kollman, *J. Comput. Chem.*, 1992, **13**, 952–962.

90 R. J. Loncharich, B. R. Brooks and R. W. Pastor, *Biopolymers*, 1992, **32**, 523–535.

91 D. R. Roe and T. E. Cheatham, *J. Chem. Theory Comput.*, 2013, **9**, 3084–3095.

92 J. L. Abascal and C. Vega, *J. Chem. Phys.*, 2005, **123**, 234505.

93 C. Vega and J. L. F. Abascal, *Phys. Chem. Chem. Phys.*, 2011, **13**, 19663–19668.

94 C. Vega, J. L. F. Abascal, M. M. Conde and J. L. Aragones, *Faraday Discuss.*, 2009, **141**, 251–276.

95 J. Wang, R. M. Wolf, J. W. Caldwell, P. A. Kollman and D. A. Case, *J. Comput. Chem.*, 2004, **25**, 1157–1174.

96 A. Jakalian, D. B. Jack and C. I. Bayly, *J. Comput. Chem.*, 2002, **23**, 1623–1641.

97 G. A. Tribello, M. Bonomi, D. Branduardi, C. Camilloni and G. Bussi, *Comput. Phys. Commun.*, 2014, **185**, 604–613.

98 J. Kästner and W. Thiel, *J. Chem. Phys.*, 2005, **123**, 144104.

99 A. Habartová, K. T. Valsaraj and M. Roeselová, *J. Phys. Chem. A*, 2013, **117**, 9205–9215.

100 S. E. Schwartz and W. H. White, *Adv. Environ. Sci. Eng.; (United States)*, 1981, **4**, 1–45.

101 V. Babin, C. Leforestier and F. Paesani, *J. Chem. Theory Comput.*, 2013, **9**, 5395–5403.

102 V. Babin, G. R. Medders and F. Paesani, *J. Chem. Theory Comput.*, 2014, **10**, 1599–1607.

103 S. K. Reddy, S. C. Straight, P. Bajaj, C. Huy Pham, M. Riera, D. R. Moberg, M. A. Morales, C. Knight, A. W. Götz and F. Paesani, *J. Chem. Phys.*, 2016, **145**, 194504.

104 S. S. Brown, T. B. Ryerson, A. G. Wollny, C. A. Brock, R. Peltier, A. P. Sullivan, R. J. Weber, W. P. Dubé, M. Trainer, J. F. Meagher, F. C. Fehsenfeld and A. R. Ravishankara, *Science (80-.).*, 2006, **311**, 67–70.

105 T. H. Bertram, J. A. Thornton, T. P. Riedel, A. M. Middlebrook, R. Bahreini, T. S. Bates, P. K. Quinn and D. J. Coffman, *Geophys. Res. Lett.*, 2009, **36**, 1–5.

106 T. H. Bertram and J. A. Thornton, *Atmos. Chem. Phys.*, 2009, **9**, 8351–8363.

107 W. L. Chang, S. S. Brown, J. Stutz, A. M. Middlebrook, R. Bahreini, N. L. Wagner, W. P. Dubé, I. B. Pollack, T. B. Ryerson and N. Riemer, *J. Geophys. Res. Atmos.*, 2016, **121**, 5051–5070.